Estimation of the transmission delays in the basal ganglia of the macaque monkey and subsequent predictions about oscillatory activity under dopamine depletion

Jean F Liénard, Lise Aubin, Ignasi Cos, Benoît Girard

Received: 20 July 2023 | Revised: 31 December 2023 | Accepted: 21 January 2024

DOI: 10.1111/ejn.16271

SPECIAL ISSUE ARTICLE

EJN European Journal of Neuroscience FENS WILEY

Estimation of the transmission delays in the basal ganglia of the macaque monkey and subsequent predictions about oscillatory activity under dopamine depletion

Jean F. Liénard[1] | Lise Aubin[1] | Ignasi Cos[1,2,3] | Benoît Girard[1]

[1]Sorbonne Université, CNRS, Institut des Systèmes Intelligents et de Robotique (ISIR), Paris, France

[2]Facultat de Matemàtiques i Informàtica, Universitat de Barcelona, Barcelona, Spain

[3]Serra-Hunter Fellow Program, Barcelona, Spain

Correspondence
Benoît Girard, Sorbonne Université, CNRS, Institut des Systèmes Intelligents et de Robotique (ISIR), 75005 Paris, France.
Email: benoit.girard@isir.upmc.fr

Funding information
Agence Nationale de la Recherche, Grant/Award Numbers: ANR-09-EMER-005-01, ANR-11-IDEX-0004-02, ANR-11-LABX-65; HORIZON EUROPE Marie Sklodowska-Curie Actions, Grant/Award Number: IF-656262; Generalitat de Catalunya, Grant/Award Number: Serra-Hunter Fellow Program

Edited by: Yoland Smith

Abstract

The timescales of the dynamics of a system depend on the combination of the timescales of its components and of its transmission delays between components. Here, we combine experimental stimulation data from 10 studies in macaque monkeys that reveal the timing of excitatory and inhibitory events in the basal ganglia circuit, to estimate its set of transmission delays. In doing so, we reveal possible inconsistencies in the existing data, calling for replications, and we propose two possible sets of transmission delays. We then integrate these delays in a model of the primate basal ganglia that does not rely on direct and indirect pathways' segregation and show that extrastriatal dopaminergic depletion in the external part of the globus pallidus and in the subthalamic nucleus is sufficient to generate β-band oscillations (in the high part, 20–35 Hz, of the band). More specifically, we show that D2 and D5 dopamine receptors in these nuclei play opposing roles in the emergence of these oscillations, thereby explaining how completely deactivating D5 receptors in the subthalamic nucleus can, paradoxically, cancel oscillations.

KEYWORDS
basal ganglia, computational model, oscillatory activities, Parkinson's disease

1 | INTRODUCTION

The basal ganglia (BG) is a set of interconnected subcortical nuclei that contains numerous internal loops (Figure 1) and that participates in large cortico-baso-thalamo-cortical loops. Unsurprisingly, the BG is subject to oscillatory phenomena in both normal and pathological conditions (Brittain & Brown, 2014; Gatev et al., 2006).

In general, the generation of oscillations in a system requires inhibitory loops, with strong enough coupling

Abbreviations: BG, basal ganglia; CM/Pf, centromedian and parafascicular thalamic nuclei; CSN, cortico–striatal neurons; Ctx, cortex; DA, dopamine; DBS, deep brain stimulation; ECoG, electrocorticography; FSI, fast-spiking interneurons; GABA, gamma aminobutyric acid; GPe, external globus pallidus; GPi, internal globus pallidus; LFP, local field potential; MEG, magneto encephalography; MPTP, 1-methyl-4-phenyl-1,2,3,6-tetrahydropyridine; MSN, medium spiny neuron; PD, Parkinson's disease; PSP, post synaptic potential; PTN, pyramidal tract neurons; STN, subthalamic nucleus; Str, striatum.

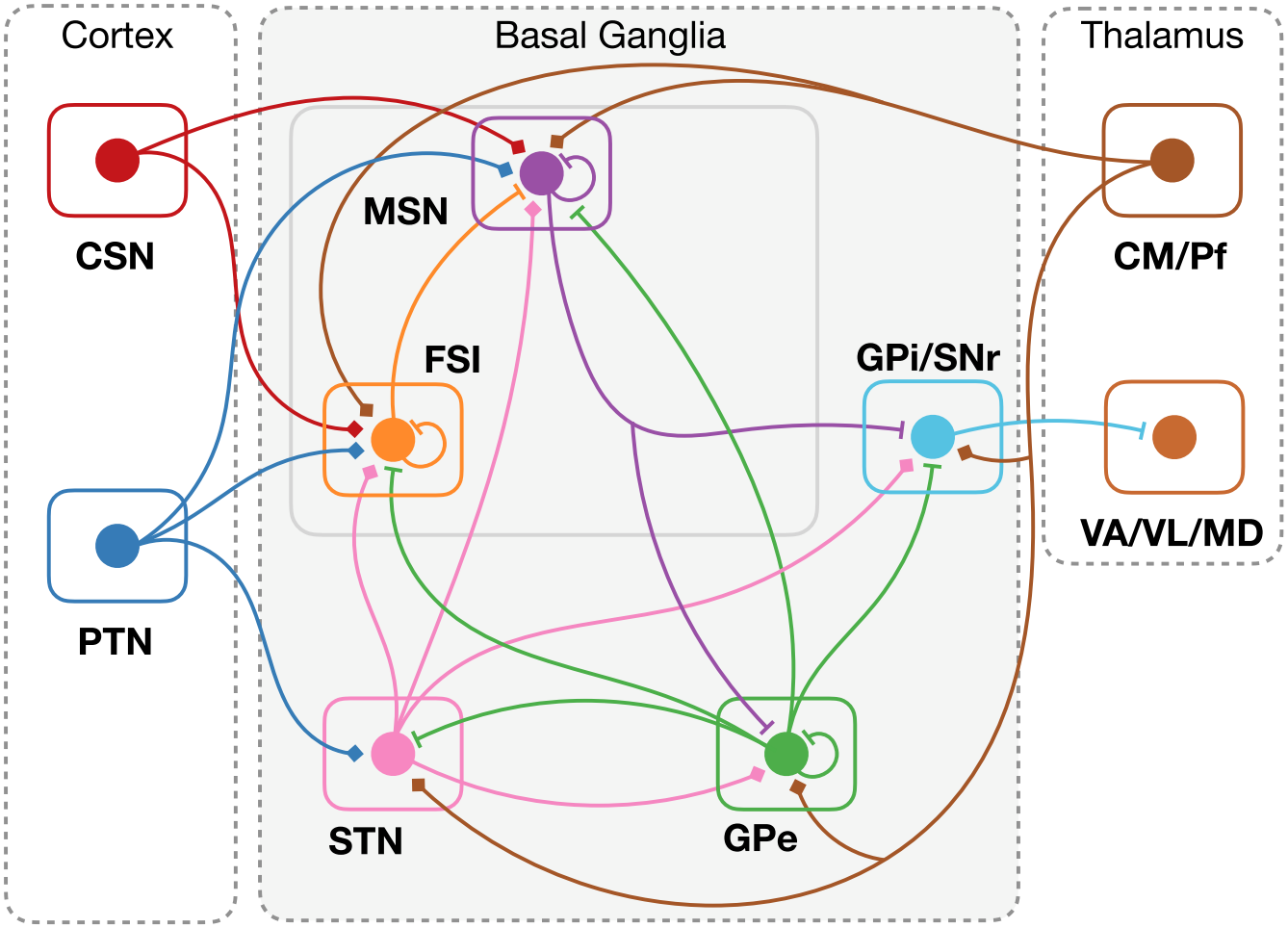

FIGURE 1 The simulated populations of the Liénard and Girard (2014) basal ganglia model (grey explicitly simulated: the cortico-striatal neurons (CSN), the pyramidal tract neurons (PTN) and the centro-median/parafascicular neurons (CM/pf) are external inputs; the ventro-anterior, ventro-lateral and medio-dorsal neurons of the thalamus (VA/VL/MD) are the targets of the GPi/SNr output of the model. Diamond projections are excitatory, and flat projections are inhibitory. All figures are by Girard et al. (2024) and are available under a CC-BY4.0 licence (https://doi.org/10.6084/m9.figshare.21131911).

gains between the loops' elements. The frequencies at which these loops oscillate depend on the time constants of the elements of the loop, as well as on the transmission delays between these elements. Concerning these transmission delays, computational models of the BG have been using very different parameterisations (see Table 1 for the delays of eight different primate BG models), which may thus result in very different predictions.

In order to inform computational models of the primate BG with plausible transmission delays, we estimate them based on 10 studies (Iwamuro et al., 2009, 2017; Kita et al., 2004, 2006; Nambu et al., 2000, 2002; Polyakova et al., 2020; Tachibana et al., 2008; Turner & DeLong, 2000; Yoshida et al., 1993) that provide the latency of the excitatory and inhibitory events in all the BG following stimulations applied in the cortex, the striatum, the subthalamic nucleus or the external globus pallidus. The combination of all these data reveals some possibly contradictory measurements, leading us to use two sets of delays. The first one is the best possible compromise that can be established when trying to satisfy all the—possibly contradictory—constraints, whereas the second one is obtained by removing the data from a single study, so as to minimise experimental data incompatibilities.

As the Liénard and Girard (2014) model was designed to estimate as best as possible the synaptic couplings between the different BG populations in monkeys, we insert the found transmission delays in this model to examine the resulting dynamics. We show that in normal conditions, its power spectrum reveals a broad peak in the high part of the β-band (20–35 Hz). We also test its reaction to dopamine depletion in the often overlooked extrastriatal neural populations. By varying the only two

TABLE 1 Axonal delays in ms from previous computational studies of the primate BG and obtained with our model and fitting method.

Connection	A	B	C	D	E	F	G	H	Cmpr	Antdrm	Antdrm2	NoPlkv
Ctx → Str	6	2	4	—	—	—	2.5	—	**6**	**9**	**9**	**9**
Ctx → STN	5	1	1	—	—	5.5	2.5	—	**4**	**4**	**4**	**4**
Str → GPe	—	1	3	—	—	—	7	—	**8**	**4**	**5**	**6**
Str → GPi	10	1	3	—	—	—	7	—	**11**	**8**	**8**	**8**
STN → GPe	—	1	1	6	5	6	2	5	**9**	**4**	**9**	**2**
STN → GPi	5	1	1	—	—	—	4.5	—	**4**	**4**	**4**	**4**
GPe → STN	—	1	1	6	5	6	1	5	**1**	**2**	**1**	**7**
GPe → GPi	—	1	1	—	—	—	3	—	**1**	**4**	**1**	**3/4**

Note: — (not applicable) indicates connections excluded from a given model. Cmpr, compromise solution; Antdrm, solution with antidromic Str → Ctx activations; Antdrm2, solution with antidromic Str → Ctx and Str → STN activations; no-Plkv, solution without the data from Polyakova et al. (2020); see text for more details. A, Leblois et al. (2006); B, Van Albada and Robinson (2009); C, Tsirogiannis et al. (2010); D, Holgado et al. (2010); E, Kumar et al. (2011); F, Pavlides et al. (2015); G, Lindahl and Hellgren Kotaleski (2016); H, Shouno et al. (2017).

free parameters of the model, we show that as the level of extrastriatal DA transits below a critical boundary, the STN–GPe network starts oscillating in high-β. Specifically, our model of the BG shows that D2 dopamine receptors in the STN and the GPe and D5 dopamine receptors in the STN play opposing roles in the emergence of extrastriatal-generated β-band oscillations.

2 | RESULTS

2.1 | Transmission delays in the primate BG

The method we used to estimate the delays between nuclei was based on an exhaustive search, tailored to reproduce the timings recorded during stimulation experiments. All delay combinations were evaluated (taking delay values in the 1–12 ms interval), and the latency of an experimentally measured inhibitory or excitatory event was simply compared to the sum of the transmission delays and neural processing time in all the possible pathways and resulted in a score dependent on the difference between the measurement and the closest pathway prediction (for more details, see Section 4.1). This operation yielded the first set of best-fitting axonal delays shown in Table 1, in the column labelled *Cmpr*. The first observation deriving from the comparison of the predicted excitation and inhibition events with the data gathered from the experimental stimulation studies (Figure 2a) is that this set of delays predicts an unreported inhibitory event in the STN, after a cortical stimulation. This early inhibition however happens 18 ms after stimulation, only 1 ms before the expected late excitation event, and could therefore be masked by the latter and be experimentally undetectable. Indeed, inhibitory events are detected when the firing rate drops below the mean firing rate minus 1.5 standard deviation, for at least two consecutive 1 ms bins (Polyakova et al., 2020).

We can observe that the set of event timings reported in Polyakova et al. (2020) has some specificities that impose strong constraints on the results of our search (see Table 2): it is the only work, where event latencies caused by striatal and GPe stimulations were measured. In particular, GPe stimulations elicited an extremely fast (as it could begin immediately after the stimulation artifact) early inhibition effect,[1] and striatal stimulations elicited an early excitation, after 4.6 ms on average. The first effect can be mediated by the direct GPe → STN connection, and indeed such a fast inhibition could not reasonably be the result of a polysynaptic pathway. This thus forces the delay of this projection to take the minimal possible value considered, 1 ms. Using such a short delay here has of course repercussions on a number of the latencies of the excitatory and inhibitory events predicted by the model (Figure 2a). Those, whose pathway use this projection, tend to be in the lower ranges: either close to the average minus one standard deviation (Ctx → GPi late excitation, Str → STN inhibition, Str → GPe excitation, and GPe → GPi excitation) or even lower (Str → GPi excitation).

The second effect, that is the STN excitation following a striatal stimulation in less than 5 ms, seems to be in contradiction with previous data. The shortest pathway supporting this effect within the BG is the Str → GPe → STN one. But the results of Kita et al. (2006) and Yoshida et al. (1993) suggest that the Str → GPe pathway has an average latency of 10 ms, implying that the Str → GPe → STN pathway should be

[1]Note that (Nambu et al., 2000) also reported, after a STN stimulation, a 1.0 ms antidromic activation in one GPe neuron.

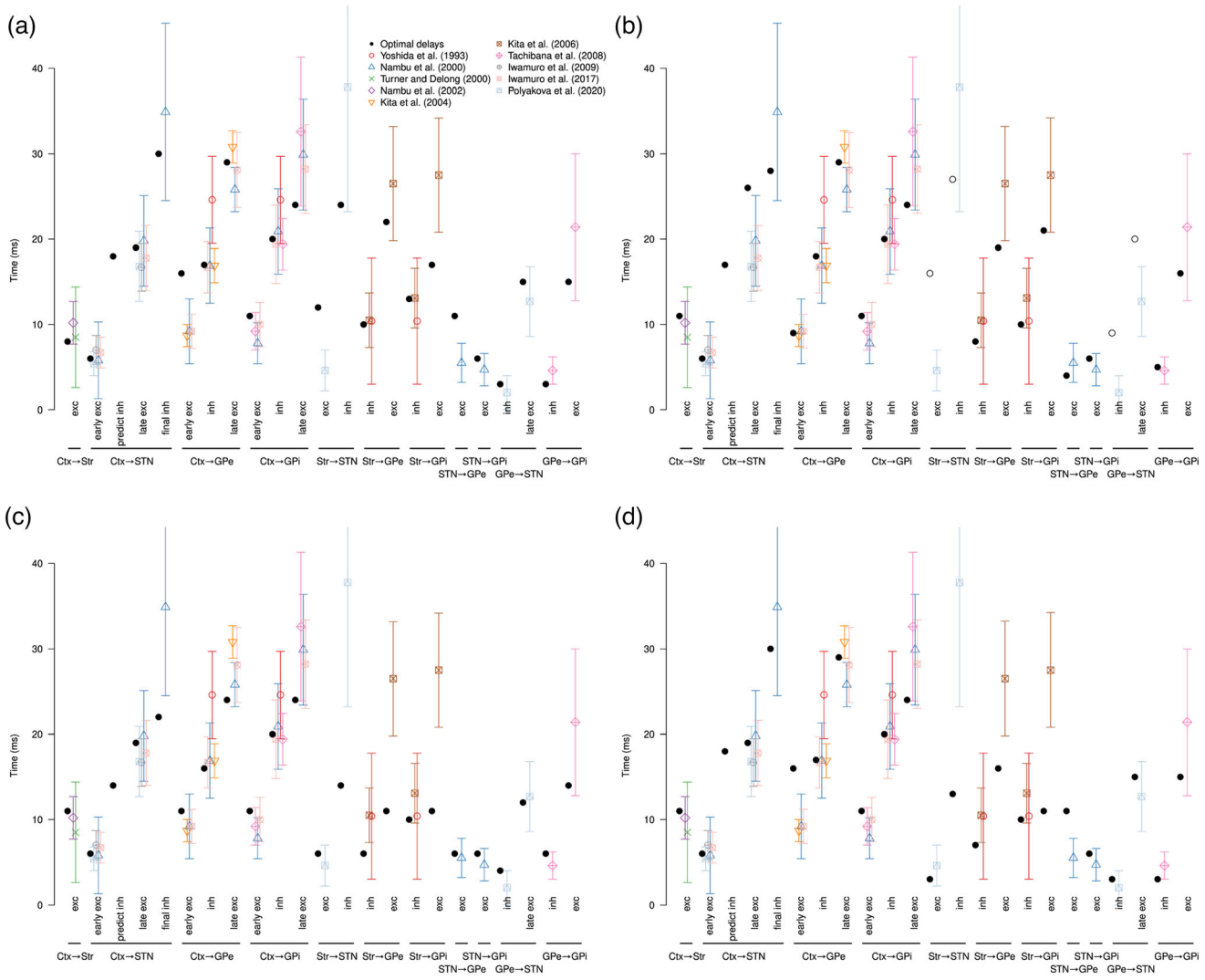

FIGURE 2 Comparison of the latencies of the excitatory and inhibitory effects measured after the stimulations (averages and standard deviations) from our set of reference studies, with those predicted by the three considered sets of delays. (a) Compromise solution based on all the studies (Cmpr set). (b) Solution obtained after exclusion of the (Polyakova et al. (2020) data (NoPlkv); the white circles are the latencies that were excluded from the optimisation. (c) Solution obtained when allowing for antidromic activations of the cortex after striatum stimulation (Antdrm). (d) Solution obtained when allowing for antidromic activations of the STN after striatum stimulation (Antdrm2).

longer than that, and is thus not compatible with a twice smaller total latency. A pathway through the thalamus, not included in the search we performed, would not solve the apparent contradiction: It would be a Str → GPi → Th → STN pathway that goes trough the Str → GPi connection, whose latency (Kita et al., 2006; Yoshida et al., 1993) is also larger than 10 ms.

This first set of delays thus appears to be the best possible compromise (*Cmpr* column in Table 1) to reconcile these two new short-latency events presented in (Polyakova et al., 2020) with the previously available data but is yet not fully satisfactory.

One possibility, to solve the apparent contradiction concerning the early Str → STN excitation, would be to find another pathway to handle this effect. We explored the possibility that this observation would result from an antidromic activation of the cortex, which would then excite the STN. Including this new pathway in the search resulted in the *Antdrm* set of delays (Table 1 and Figure 2c). This second set of delays now predicts an early Ctx → STN inhibition that should be detectable, as it happens 5 ms before the documented late excitation. Moreover, while using this antidromic pathway allows the Str → STN excitatory event latency to fit nicely in the expected interval, it is also recruited to explain the Str → STN inhibitory event, the Str → GPe excitatory event and the Str → GPi excitatory event, causing these latencies to become quite low (almost two standard

TABLE 2 Summary of the candidate pathways and reference data in ms (Part 1).

Stim.	Rec.	Response	Candidate pathways	Latency (ms)
Str	GPe	Inhibition	Str → GPe	10.5 ± 3.2[a] 10.4 ± 7.4[b]
		Excitation	Str → GPe → STN → GPe (Ctx ↞ Str antidromic); Ctx → STN → GPe (STN ↞ Str antidromic); STN → GPe	26.5 ± 6.7[a]
	GPi	Inhibition	Str → GPi	13.1 ± 3.5[a] 10.4 ± 7.4[b]
		Excitation	Str → GPe → STN → GPi (Ctx ↞ Str antidromic); Ctx → STN → GPi (STN ↞ Str antidromic); STN → GPI	27.5 ± 6.7[a]
	STN	Excitation	Str → GPe → STN (Ctx ↞ Str antidromic); Ctx → STN (STN ↞ Str antidromic)	4.6 ± 2.4[c]
		Inhibition	Str → GPe → STN → GPe → STN (Ctx ↞ Str antidromic); Ctx → STN → GPe → STN (STN ↞ Str antidromic); STN → GPe → STN	37.8 ± 14.6[c]
STN	GPe	Excitation	STN → GPe	5.5 ± 2.3[d]
	GPi	Excitation	STN → GPi	4.7 ± 1.9[d]
GPe	GPi	Inhibition	GPe → GPi GPe → STN → GPi	4.6 ± 1.6[e]
		Excitation	GPe → STN → GPe → GPi GPe → STN → GPe → STN → GPi	21.4 ± 8.6[e]
	STN	Inhibition	GPe → STN	2.0 ± 2.0[c]
		Excitation	GPe → STN → GPe → STN	12.7 ± 4.1[c]

Note: The column 'Stim.' indicates the location of the stimulation; 'Rec.' indicates the location of the recording; 'Response' indicates the type of response recorded; the candidate pathways along the quantitative data expressed as mean ± SD constitute the remainder of the table. In the case of striatal stimulation, we also consider pathways involving antidromic excitation of cortical or STN axons, noted as 'Ctx ↞ Str antidromic' and 'STN ↞ Str antidromic' (see Section 5 for details).

[a]Kita et al. (2006).
[b]Yoshida et al. (1993).
[c]Polyakova et al. (2020).
[d]Nambu et al. (2000).
[e]Tachibana et al. (2008).

deviations away from the averages documented in the experimental data). The introduction of this hypothesis of antidromic activation is thus not satisfactory, as it solves some problems but simultaneously introduces new ones.

Another possibility to solve the same problem would be to consider the possible direct antidromic activation of the STN by striatal stimulation. The set of delays obtained when adding this possibility to the search is reported under the name *Antdrm2* (Table 1 and Figure 2d). This new set has similar problems to the *Antdrm* one: It causes the Str → STN inhibitory event and the late Str → GPe and Str → GPi excitatory events to happen much earlier than required.

Finally, we searched what would be the best set of transmission delays if we discarded the data from Polyakova et al. (2020). The resulting set (*NoPlkv* column in Table 1, Figure 2b) also predicts a detectable inhibitory event in the STN after cortical stimulation, as it happens 9 ms before the late excitatory event. The other limitations of this third set of delays are as follows: the conjunction of a Ctx → STN late excitation latency that is a bit too large, whereas the following final inhibition is a bit too low; Str → GPe and → GPi excitation latencies that are also in the lower range. On this restricted set of data, it scores better than the Cmpr set but is also not fully satisfactory.

As such, in the remainder of the article, we will both use the Cmpr and the NoPlkv sets and thus duplicate all simulations.

Many previous computational studies assumed the STN → GPe and GPe → STN axonal delays to be similar

or equal (Table 1). By contrast, all our candidate explanations yield largely different delays for these projections in the three considered delay sets. Surprisingly, the *Cmpr* set and the *NoPlkv* set have opposite tendencies: the STN → GPe is the slowest projection (9 ms) according to the *Cmpr* set, whereas it is the GPe → STN (7 ms) according to the *NoPlkv* one.

An intuitive explanation for the imbalance of these two delays inside the same loop may be gained by observing the timing of the early excitation of GPe after cortical stimulation (recorded after roughly 9 ms in Nambu et al., 2000, Kita et al., 2004, cf. Table 3). The quick early excitation of GPe is most likely to be conveyed through the Ctx → STN → GPe pathway, since the alternative pathway Ctx → Str → GPe → STN → GPe involves several other loops and is incompatible with other timings. Furthermore, given that the Ctx → STN connection conveys excitatory events in about 6–7 ms (Iwamuro et al., 2009, 2017; Nambu et al., 2000; Polyakova et al., 2020), the STN → GPe connection delay has to be around 2–3 ms. Intuitively, such a quick STN → GPe connection implies a slow GPe → STN connection in order to satisfy the other timing constraints within the BG (Tables 3 and 2). For example, the Ctx → GPe, the Str → GPe, the Str → GPi and GPe → GPi late excitatory events all transit through the STN ↔ GPe loop. This is indeed what the *NoPlkv* set predicts. Mechanistically, this delay imbalance is consistent with the potential myelination of glutamatergic STN axons. Corroborative with the *NoPlkv* set, evidence of the existence of STN axon myelination has been reported in monkey and rat studies (Koshimizu et al., 2013; Yelnik & Percheron, 1979). Incidentally, a detailed computational study of STN neurons has shown that their myelination may mediate the therapeutic effects of deep brain stimulation (Bellinger et al., 2008). On the contrary, and as previously mentioned, the *Cmpr* set is heavily constrained by the minimal GPe → STN latency required

TABLE 3 Summary of the candidate pathways and reference data (Part 2).

Stim.	Rec.	Response	Candidate pathways	Latency (ms)
Ctx	Str	Excitation	Ctx → Str	10.2 ± 2.5[a] 8.5 ± 5.9[b]
	STN	Early exc.	Ctx → STN	5.8 ± 4.5[c] 7.0 ± 1.7[d] 6.7 ± 1.8[e] 5.4 ± 1.4[f]
		Late exc.	Ctx → Str → GPe → STN Ctx → STN → GPe → STN → GPe → STN	19.8 ± 5.3[c] 16.7 ± 2.8[d] 17.8 ± 3.8[e] 16.8 ± 4.1[f]
		Final inhib	Ctx → Str → GPe → STN → GPe → STN Ctx → STN → GPe → STN	32.3 ± 11.8[c]
	GPe	Early exc.	Ctx → Str → GPe → STN → GPe Ctx → STN → GPe	9.2 ± 3.8[c] 8.7 ± 1.3[g] 9.2 ± 2.0[e]
		Inhibition	Ctx → Str → GPe Ctx → STN → GPe → STN → GPe	16.9 ± 4.4[c] 16.9 ± 2.0[g] 24.6 ± 5.1[h] 16.7 ± 3.0[e]
		Late exc.	Ctx → Str → GPe → STN → GPe Ctx → STN → GPe Ctx → STN → GPe → STN → GPe → STN → GPe	25.8 ± 2.6[c] 30.8 ± 1.9[g] 28.1 ± 4.4[e]

Note: See Table 2 for notations.
[a]Nambu et al. (2002).
[b]Turner and DeLong (2000).
[c]Nambu et al. (2000).
[d]Iwamuro et al. (2009).
[e]Iwamuro et al. (2017).
[f]Polyakova et al. (2020).
[g]Kita et al. (2004).
[h]Yoshida et al. (1993).

by the (Polyakova et al., 2020) data, such that the STN → GPe delay is used to compensate and prolong the duration of the transit of the signals inside the STN ↔ GPe loop.

2.2 | Conditions for the emergence of β-band oscillations

Having determined two plausible sets of estimates of the transmission delays in the rhesus monkey BG, we insert them in a model built so as to estimate the coupling between the BG populations of the same species (Liénard & Girard, 2014). Both the *Cmpr*- and the *NoPlkv*-based models (Figure 3) produce power spectra, which, in the STN, GPe and GPi, exhibit a wide bump of preferential frequencies covering the whole β- and lower γ-bands, centered on the high part (20–35 Hz) of the β-band.

Concerning the influence of dopaminergic depletion on these dynamics, we focused on the role of extrastriatal dopaminergic receptors. This is because, first, earlier models of the emergence of oscillatory activity in Parkinson's disease (Gillies et al., 2002; Terman et al., 2002) highlighted the role of the extrastriatal circuitry of the BG (and in particular of the GPe–STN loop). Second, this is because the strong overlap between the direct and indirect pathways in monkeys (Lévesque & Parent, 2005; Parent et al., 1995) probably limits the differential effects D1 and D2 medium spiny neurons (MSNs) exert on the rest of the circuit. Finally, and more importantly, this is because experimental results (Benazzouz et al., 2014) also highlight the involvement of extrastriatal receptors in Parkinson's disease.

We simulated the effect of extra-striatal DA depletion on both the pre-synaptic D2-like receptors in the GPe and the STN and the post-synaptic D5 receptors in the STN (See Equations 10 and 11) while incorporating the axonal delays described in the previous section. Our results show that an increase of the PSP amplitude in the GPe and the STN and a not-too-strong increase of the mean threshold between resting and firing rates in the GPe and the STN generate an oscillatory regime for both sets of delays (dark-blue regions of the parameter exploration matrices of Figures 4a and 5a). This oscillatory regime affects all the simulated populations (Figure 6), and because of the fundamental differences in the transmission delays in the STN ↔ GPe loop for the two considered sets of delays, the STN peak activity precedes the GPe one (Figure 6, 'GPe & STN' panels) with a longer duration with the *Cmpr* one (11 ms) than with the NoPlkv one (3 ms). The frequencies of these oscillations are in the upper β-band (20–35 Hz), with an average frequency of 32 Hz for the *Cmpr* set of delays and 35 Hz for the *NoPlkv* one (panels B of Figures 4 and 5). It is interesting to note that in the normal regime of operation (power spectra in Figures 4c and 5c), the tendency of the model to favour these frequencies is already visible.

The conditions of generation of a high-β oscillatory behaviour in the STN and the GPe, when simulating extra-striate dopaminergic depletion, require a trade-off between the facilitation of the PSP, driven by the D2 receptors and the weakening of the STN excitability by the D5 receptors.

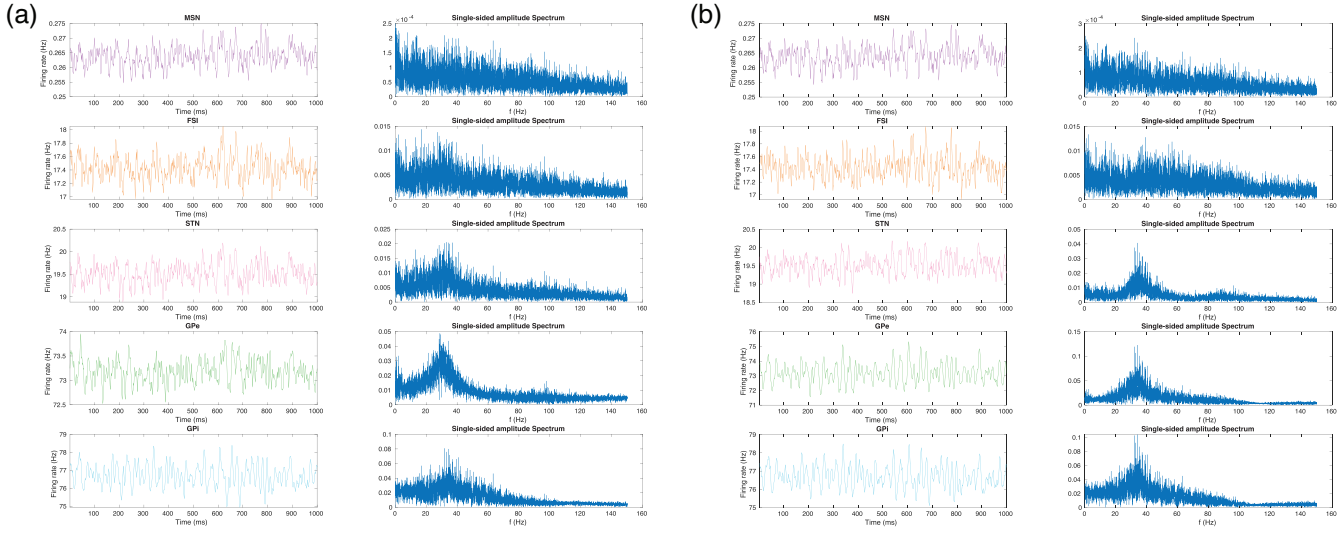

FIGURE 3 Simulated activity and power spectra of all neural populations, in normal conditions, at rest. These illustrative simulations use the parameterisation #2 of the BCBG. (a) With the Cmpr set of delays. (b) With the NoPlkv set of delays. The colour code, identical to the one used in Figure 1, identifies the neural populations.

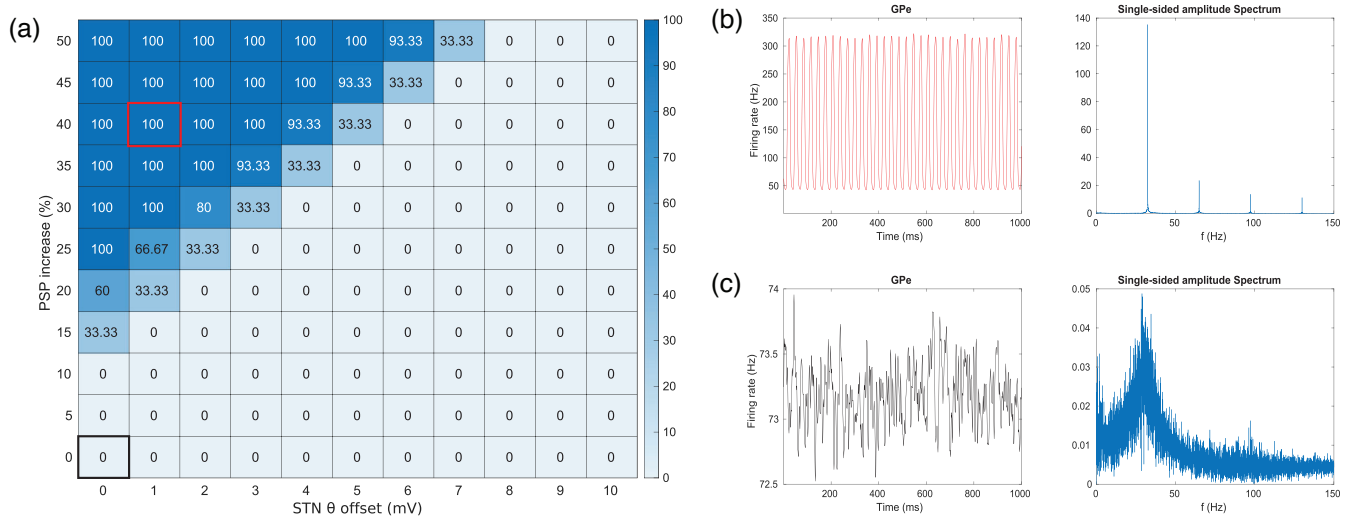

FIGURE 4 Emergence of oscillations under dopamine depletion with the Cmpr set of delays. (a) Proportion of. The basal ganglia models that oscillate depending on the increase in the PSPs in the GPe and STN (D2 receptors) and on the increase in the firing threshold of the STN (D5 receptors). (b) Oscillatory GPe activity (left) and the corresponding power spectrum (right) corresponding to a PSP increase of 40% and an STN threshold increase of 1 mV (shown with a red square in (a). (c) Irregular GPe activity (left) and the corresponding power spectrum (right) corresponding to the model without dopamine depletion (shown with a black square in (a).

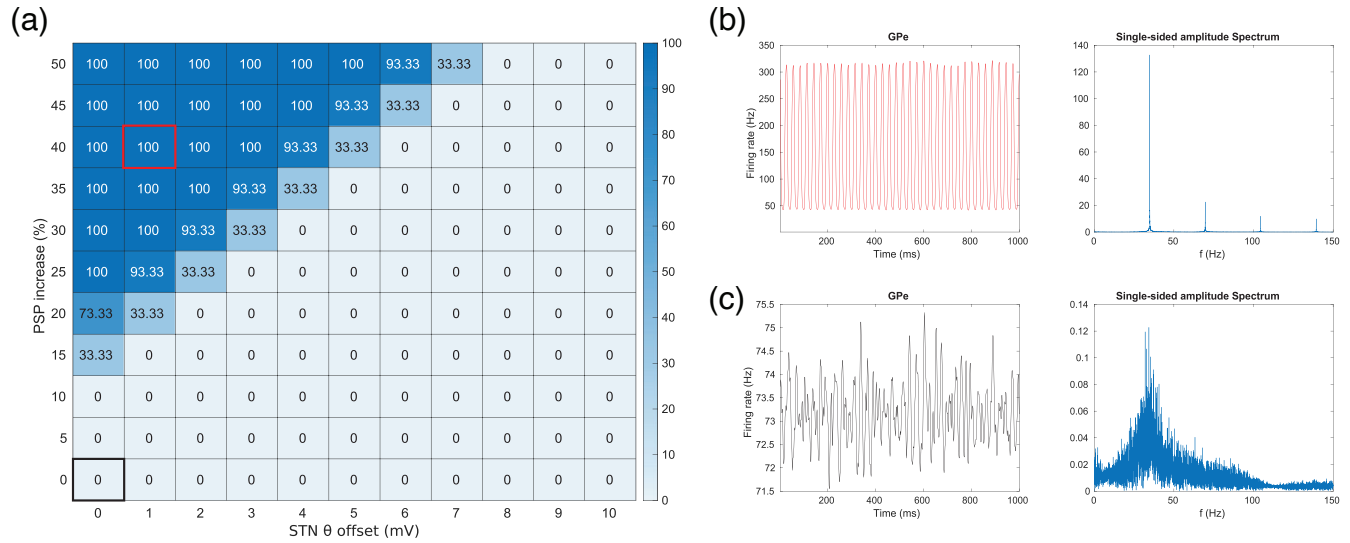

FIGURE 5 Emergence of oscillations under dopamine depletion with the NoPlkv set of delays. (a) Proportion of the basal ganglia models that oscillate depending on the increase in the PSPs in the GPe and STN (D2 receptors) and on the increase in the firing threshold of the STN (D5 receptors). (b) Oscillatory GPe activity (left) and the corresponding power spectrum (right) corresponding to a PSP increase of 40% and an STN threshold increase of 1 mV (shown with a red square in (a). (c) Irregular GPe activity (left) and the corresponding power spectrum (right) corresponding to the model without dopamine depletion (shown with a black square in (a).

It is worth noting that although our simulations of DA depletion also reported oscillatory activity in other nuclei, such as the GPi and the striatum, including MSN and FSI cells (Figure 6), these oscillations did not originate locally. Replacing the simulated pallido-striatal and subthalamo-striatal activities with synthetic signals mimicking the baseline obtained in the normal condition, cleared the striatal oscillator activity (Figures 7 and 8, 'no feedback to striatum' panels), thus confirming the GPe ↔ STN origin of the oscillations. By contrast, if the GPe → FSI connection remained active (see Figures 7 and 8, 'GPE → FSI enabled' panels), the oscillations re-emerged in the striatum, showing that this connection is a critical relay for the propagation of these oscillations in the striatum. Note also that keeping this feedback connection active, and thus the

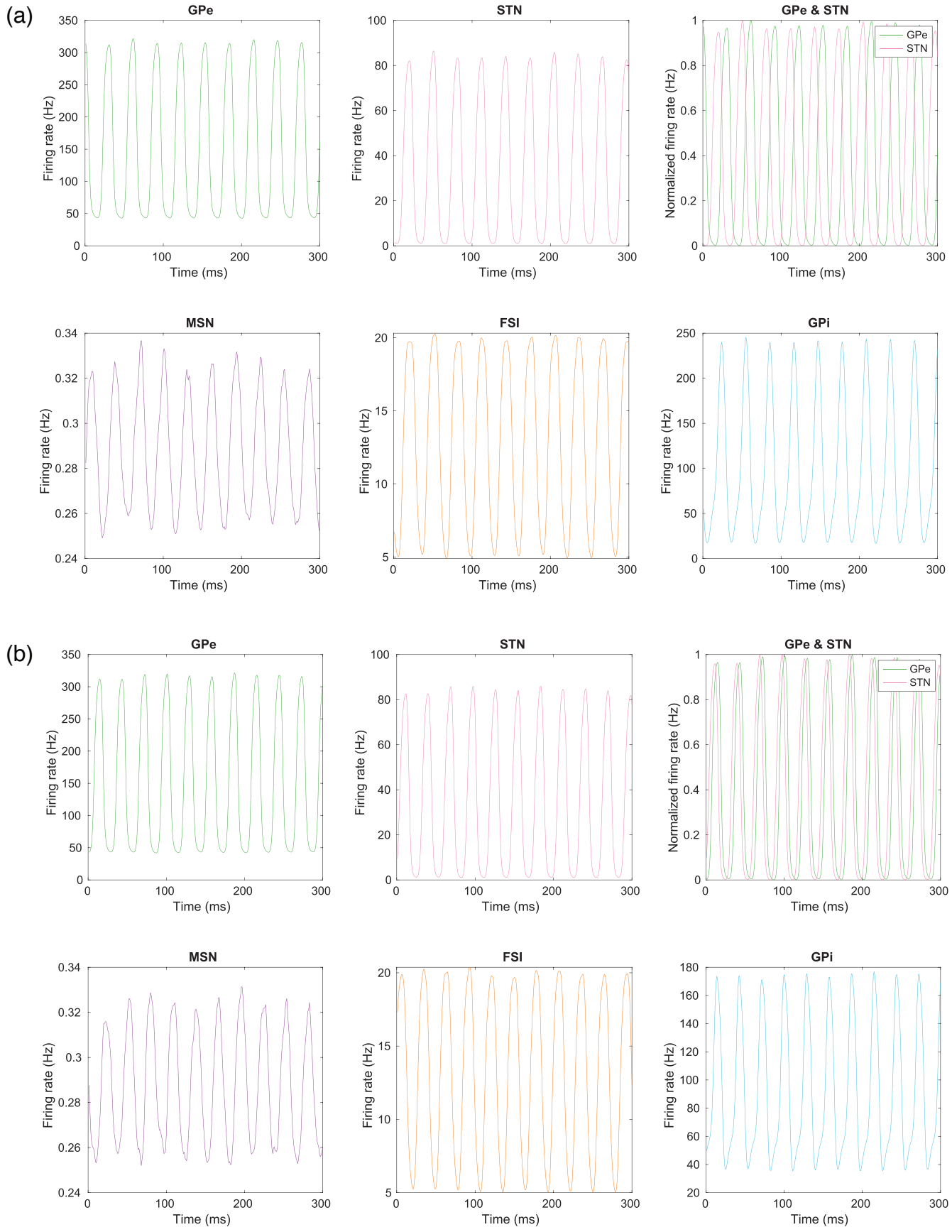

FIGURE 6 Legend on next page.

FIGURE 6 Oscillatory activity in the whole basal ganglia circuit, caused by DA depletion. These illustrative simulations use parameterisation #2 of the BCBG, a GPe and STN PSP increase of 40% and an STN firing threshold increase of 1 mV. (a) With the Cmpr set of delays. (b) With the NoPlkv set of delays. The colour code, identical to the one used in Figure 1, identifies the neural populations.

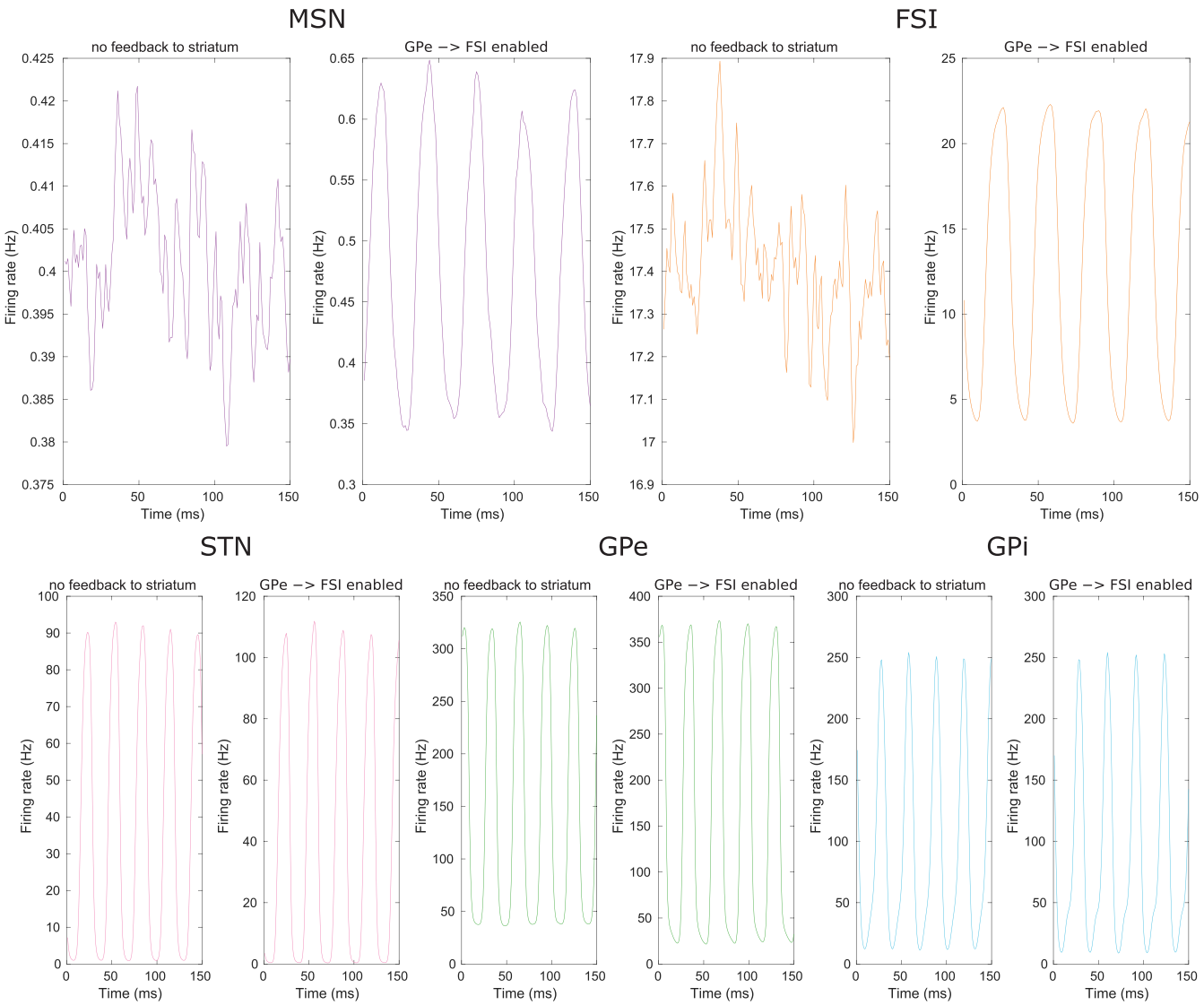

FIGURE 7 Transmission of the oscillations in the circuit (Cmpr set of delays, BCBG model parameterisation #2, 40% GPe and STN input PSP increase, 1 mV STN threshold increase). In the first set of simulations (left part of each panel), the feedback from the GPe and the STN to the striatum was overridden: STN and GPe input were replaced by synthetic inputs mimicking the normal GPe and STN activities. In the second set of simulations (right part of each panel), the GPe → FSI feedback was selectively re-activated. Oscillations in the MSNs and the FSIs appear only in the second set of simulations, showing that striatal oscillations are the byproduct of GPe–STN oscillations mediated selectively through the GPe → FSI connection.

MSN → GPe → FSI → MSN loop intact, increased the amplitude of the oscillations in the GPe and the GPi. The GPi provides no input to other BG nuclei and thus cannot be involved in the observed emergence of oscillations. In conclusion, oscillatory activity in the striatum and GPi does not originate locally but is conveyed from the phase-locked oscillatory activity of the GPe ↔ STN loop.

The frequency of the oscillations depended essentially on the projection delays between the GPe and the STN. We explored, for both sets of delays, the changes in oscillation frequency caused by all possible variations of the GPe → STN and the STN → GPe delays between 1 and 13 ms (Figure 9) while keeping the rest identical: The sum of these delays clearly defines the oscillation frequency.

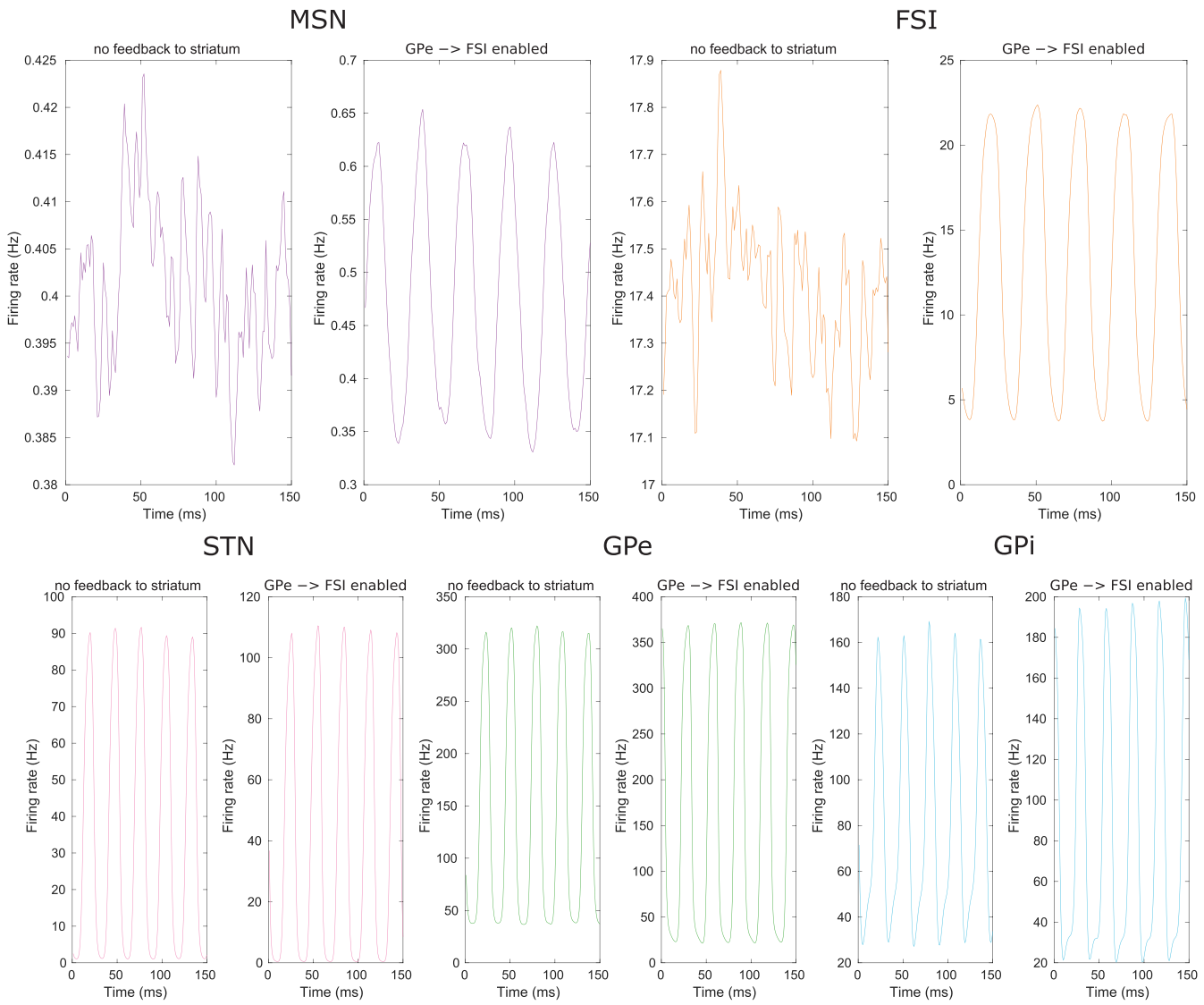

FIGURE 8 Transmission of the oscillations in the circuit (NoPlkv set of delays, BCBG model parameterisation TN input PSP increase, 1 mV STN threshold increase). In the first set of simulations (left part of each panel), the feedback from the GPe and the STN to the striatum was overridden: STN and GPe input were replaced by synthetic inputs mimicking the normal GPe and STN activities. In the second set of simulations (right part of each panel), the GPe → FSI feedback was selectively re-activated. Oscillations in the MSNs and the FSIs appear only in the second set of simulations, showing that striatal oscillations are the byproduct of GPe–STN oscillations mediated selectively through the GPe → FSI connection.

3 | DISCUSSION

This study has proposed a simple method to combine the existing stimulation experiments used to measure the latency of excitatory and inhibitory events in the macaque monkey BG, so as to estimate the transmission delays in the various connections of the circuit. This method highlighted some apparent contradictions in the experimental data concerning the GPe to STN projection, which led us to propose two sets of delays, a first one providing the best possible compromise resulting from this data, and a second one ignoring the measures obtained in the Polyakova et al. (2020) study that introduced the potential contradiction (columns *Cmpr* and *NoPlkv* in Table 1, respectively).

We have also shown that specific changes in biophysical properties within the GPe–STN loop are sufficient to trigger oscillations in the high β-band (20–35 Hz). These predictions resulted from the introduction of these sets of delays within a computational model of the macaque monkey BG, fitted from over a hundred independent anatomical and physiological experimental data (Liénard &

STN → GPe

GPe → STN (Osc. Freq. in Hz)	1 ms	2 ms	3 ms	4 ms	5 ms	6 ms	7 ms	8 ms	9 ms	10 ms	11 ms	12 ms	13 ms
1 ms	74	64	56	49	44	40	37	35	32	30	29	27	26
2 ms	64	56	49	44	40	37	35	32	30	29	27	26	25
3 ms	56	49	44	40	37	35	32	30	29	27	26	25	24
4 ms	49	44	41	37	35	32	30	29	27	26	25	24	22
5 ms	44	41	37	35	32	30	29	27	26	25	24	22	22
6 ms	41	37	35	32	30	29	27	26	25	23	22	22	21
7 ms	37	35	32	30	29	27	26	25	23	22	22	21	20
8 ms	35	32	30	29	27	26	25	24	22	22	21	20	19
9 ms	32	30	29	27	26	25	24	22	22	21	20	19	18
10 ms	30	29	27	26	25	24	22	22	21	20	19	18	18
11 ms	29	27	26	25	24	22	22	21	20	19	18	18	17
12 ms	27	26	25	23	22	22	21	20	19	18	18	17	17
13 ms	26	25	23	22	22	21	20	19	18	18	17	17	16

STN → GPe

GPe → STN (Osc. Freq. in Hz)	1 ms	2 ms	3 ms	4 ms	5 ms	6 ms	7 ms	8 ms	9 ms	10 ms	11 ms	12 ms	13 ms
1 ms	74	63	55	49	44	40	37	35	32	31	29	27	26
2 ms	63	55	49	44	40	37	35	32	31	29	27	26	25
3 ms	55	49	44	40	37	35	32	31	29	27	26	25	24
4 ms	49	44	41	37	35	32	31	29	27	26	25	24	23
5 ms	44	41	37	35	32	31	29	27	26	25	24	23	22
6 ms	41	37	35	32	31	29	27	26	25	24	23	22	21
7 ms	37	35	32	31	29	27	26	25	24	23	22	21	20
8 ms	35	33	31	29	27	26	25	24	23	22	21	20	19
9 ms	33	31	29	27	26	25	24	23	22	21	20	19	18
10 ms	31	29	27	26	25	24	23	22	21	20	19	18	18
11 ms	29	27	26	25	24	23	22	21	20	19	18	18	17
12 ms	27	26	25	24	23	22	21	20	19	18	18	17	17
13 ms	26	25	24	23	22	21	20	19	18	18	17	17	16

FIGURE 9 Frequency of oscillation (in Hz) as a function of the axonal delays between STN and GPe. Delays from STN to GPe are listed as columns and from GPe to STN as rows. The other delays are set according to the Cmpr set of delays (left) and the NoPlkv set of delays (right). The optimised axonal delays are shown in the cells marked with a black rectangle. Colours indicate different oscillation regimes, with the β-band (15–35 Hz) shown in blue and the γ-band (35–80 Hz) shown in green.

Girard, 2014). Although this model contains numerous parameters, it is important to notice that these were optimised to fit to healthy non-human primate data. By contrast, the results and predictions of this study result from varying two free parameters only, which model the process of DA depletion in GPe and STN: the D2 PSP amplification and D5 firing threshold increase (Figures 4 and 5). A first prediction of our model is that extra-striate D2 receptors (in the GPe and the STN) and D5 receptors (in the STN) play opposing roles in the generation of β-band oscillations when DA decreases: D2 receptors cause them to appear and gradually increase their intensity, and D5 receptors attenuate them. A second prediction is that decreasing the STN D5 receptor activity beyond its constitutive activity (i.e. degrade the D5 receptors' normal behaviour even stronger than with DA depletion) would shift the dynamics of the system towards a steady state with no oscillations (see Figures 4 and 5, shift from the dark-blue to the light-blue area along the horizontal 'STN θ offset' axis). This is consistent with observations by Chetrit et al. (2013), who showed that diminishing the D5 receptor constitutive activity in the STN of 6-OHDA PD rats did cancel abnormal neuronal activity and reversed motor impairment. Finally, the oscillatory activity reported in other nuclei (e.g. within the FSI-MSN circuitry) does not originate locally but is rather relayed by projections from the GPe/STN loop (Figures 7 and 8).

4 | AXONAL DELAYS

Numerous stimulation studies participated in characterising transmission delays across different neuronal groups of the BG circuitry (Iwamuro et al., 2009, 2017; Kita et al., 2004, 2005, 2006; Nambu et al., 2000, 2002; Polyakova et al., 2020; Tachibana et al., 2008; Turner & DeLong, 2000; Yoshida et al., 1993), to the best of our knowledge, this work is the first to combine these experimental studies by computational means in order to determine the set of delays that could be compatible with all of them. In a review dedicated to the GPe, Jaeger and Kita (2011) proposed in their Figure 1 a summary of the results obtained by the then-available stimulation studies, in which a set of transmission delays was proposed to explain the latencies of excitatory and inhibitory events (panel A of their Figure 1). The details of the method used to propose this set of delays were unfortunately not documented in the main text. We have evaluated the score of this set with our method (Figure 10); it clearly performs worse than the sets we report here. In particular, it tends to underestimate the latency of all the late effects. Interestingly, this set of delays also predicts an early inhibition in the STN after cortical stimulation (with a 10 ms latency), before the late excitation and the final inhibition. In the panel B of their Figure 1, they suggest that this inhibition would be sufficient to stop the STN early excitation, but may not be strong

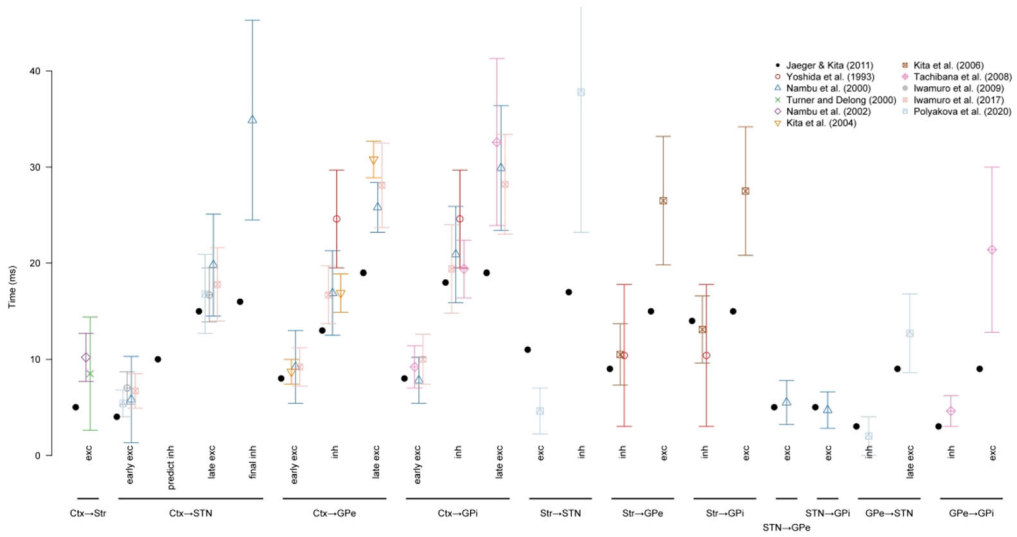

FIGURE 10 Comparison of the latencies of the excitatory and inhibitory effects measured after the stimulations (averages and standard deviations) from our set of reference studies, with those predicted by the set of delays in Jaeger and Kita (2011).

enough to generate an inhibitory event per se (i.e. a decrease of the activity below the baseline, strong enough and long enough to be categorised as an inhibitory event), explaining why it is not reported in experimental studies.

As mentioned above, the results from (Polyakova et al., 2020) raise questions that require further investigation on both the experimental and the modelling sides. First, the extremely short transmission delay from the GPe to the STN (1 ms) measured in this study imposes, in order to stay as much as possible coherent with the rest of the data, an STN to GPe delay (9 ms) that is much larger than what suggests the Nambu et al. (2000) direct measure (5.5 ± 2.3 ms). Second, the 5 ms delay between a striatal stimulation and an excitatory event in the STN does not appear to be compatible with the most obvious and shortest pathways for its transmission (Str → GPe → STN or Str → GPi → Th → STN), as they recruit projections whose transmission delay is at least 10 ms (Str → GPe or Str → GPi). However, the apparent inconsistency of these measures may purely result from the limitations of our methodology: we adopted a very crude way of estimating the total duration of the transmission of a stimulation along a pathway (summing transmission delays with neural processing delay common to all BG neural populations), which does not honour the real complexity of the dynamics of the BG neural circuit. It could be interesting in a future study to refine the estimates of delays by using distributions of delays, mimicking the skewness of the experimental statistics, rather than the average values only. We cannot also exclude the possibility that we neglected possible alternate transmission pathways, especially those that would transit outside the BG proper. A more subtle approach to model these phenomena may thus help solve these paradoxes. Nevertheless, an experimental replication of the STN recordings following striatal and GPe stimulations would be quite useful to ascertain that the sources of these potential inconsistencies come from the model.

A possibility that has not been explored in the present study is the potential existence in monkeys of the two GPe subpopulations identified in mice and rats: the prototypical and the arkypallidal ones (Guilhemsang & Mallet, 2024). The arkypallidal neurons, specifically, receive inputs from the striatal MSNs, the STN neurons and the prototypical GPe neurons, and project back to the striatum, contacting both MSNs and striatal interneurons (Figure 11). They thus have the potential to participate in the generation of late excitatory or inhibitory events in the GPe or the GPi following striatal or cortical stimulations. Only late events are concerned because these would have to transit through the striatum and thus be impacted by the latencies of the striatum to GPe or to GPi pathways (of at least 10 ms, see Table 2). The inclusion of these many pathways in our systematic search could result in an improvement of the late events that tend to be at the bottom of the acceptable intervals (Figure 2).

Too little information is available about the existence of these subpopulations in monkeys, and therefore about their potential anatomical and electrophysiological characteristics, to be able to integrate them properly in our current BG computational model. It has been proposed to

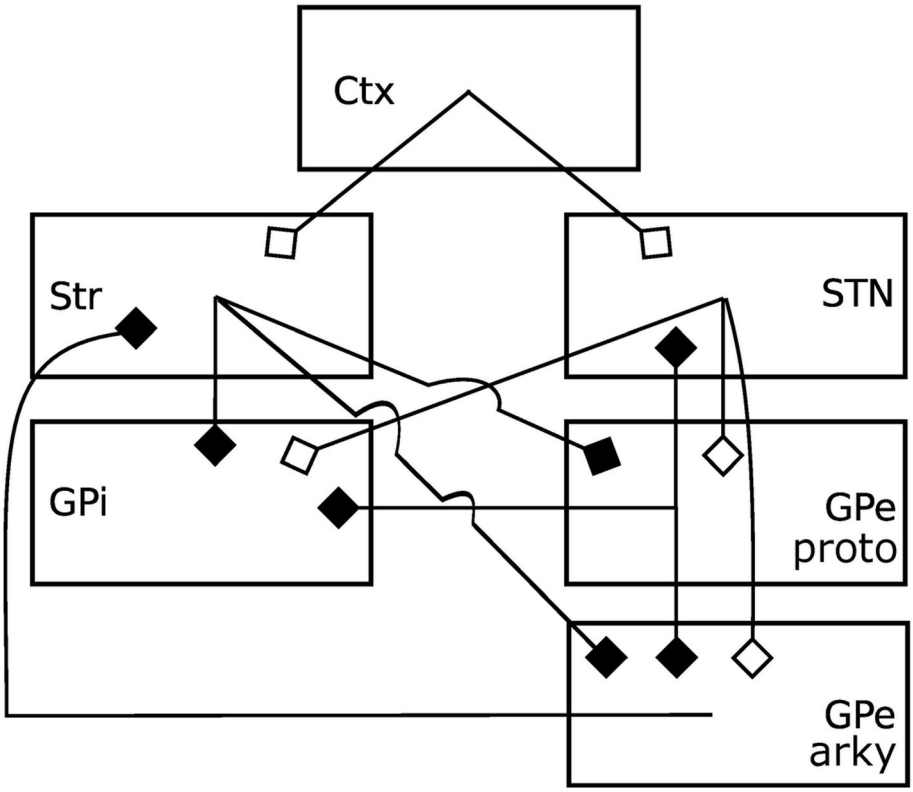

FIGURE 11 Schematical organisation of the GPe prototypical and arkypallidal populations within the basal ganglia circuitry.

identify high-frequency burst neurons with prototypical neurons and low-frequency burst neurons with arkypallidal ones (Katabi et al., 2023). This proposal has to be further experimentally explored before it can be translated into a model that requires data such as the relative number of neurons in each population, the average number of synaptic boutons of each afferent projection and so forth. Note however that our current BG computational model does include feedback connections from the GPe to the striatum (Figure 1), but the GPe is modelled as a whole. The simulated GPe activity thus represents the average activity of all GPe neurons merged together.

Finally, concerning humans, estimations of transmission delays (Oswal et al., 2016, 2021) have been performed by looking at the delays of Granger causality linking MEG signals in the cortex to LFP signals from deep brain stimulation (DBS) electrodes in the STN and the GPi, in the high and low beta ranges. These suggest that direct cortical to STN delays would be of the order of 15–20 ms, whereas indirect delays (probably through the striatum and the GPe) would be larger than 40 ms and that cortical to GPi delays would be of approximately 30 ms. It is however difficult to compare these numbers directly to those measured in monkeys by Nambu's team: The measurement is very indirect and has a larger variability. With a more direct approach (antidromic stimulations in the STN using DBS, measured with ECoG in the prefrontal cortex), Chen et al. (2020) measured a 6 ms delay between the prefrontal cortex and STN (and an extremely fast 2 ms pathway from the inferior frontal gyrus). These values are quite compatible with delay estimations in macaque monkeys.

4.1 | Striatal and extra-striatal contributions to pathology

Our results suggest that β-band oscillations may arise in the BG circuitry when DA is scarce, irrespective of the effect of DA depletion on DA receptors in the MSN and the FSI in the striatum, which our model deliberately excludes. Although the extent to which striatal cells contribute to these oscillations remains to be addressed, our results show that the direct/indirect pathway segregation may be neither central nor necessary to understand the PD oscillatory phenomena in primates.

By removing our focus from the segregation of striatal D1/D2 receptors, we implicitly assumed that the excitatory and inhibitory effects of DA in the striatum cancel each other, yielding no effect on MSN firing rate on average. Consistent with this, electrophysiological studies in primates reported no change in the striatal firing rate after MPTP injection (Goldberg et al., 2002). Furthermore, the modification of the distribution of the firing

rates in the MSN population (decreased activity in D1 neurons and increased activity in D2 ones) would exert little influence on the STN ↔ GPe loop, as a consequence of the massively collateralised striato-fugal projection in primates (Lévesque & Parent, 2005; Nadjar et al., 2006; Parent et al., 1995).

Finally, we did not model the effect of DA depletion on the GPi, first, because experimental data on the effects of such depletion is incomplete and contradictory effects have been reported (Rommelfanger & Wichmann, 2010), and second, because the GPi projects only outside the modelled BG circuitry, and thus cannot participate in the local generation of oscillations. Should the model be extended to encompass the cortico-baso-thalamo loops, the GPi would become a central actor of these loops, and as such would participate actively in their dynamics. Modelling the GPi DA receptor would then become essential to determine the effects of DA depletion across the circuit.

The expression of D5 receptors in the GPe, similar to what is found in the STN, and their effect on neural activity is unclear (Rommelfanger & Wichmann, 2010). Thus, for the sake of completeness, we simulated the same increase of the firing threshold in the GPe as in the STN. Adding that modulation only marginally modifies the reported boundaries of the oscillation region in the parameter space (Figure 12a,c). Indeed, isolating the effect of these putative GPe receptors by removing the D5 modulation in the STN revealed that increasing the firing threshold of the GPe does not really affect the emergence of oscillations. This suggests that cancelling the constitutive activity of D5 receptors in the GPe should not replicate the electrophysiological and motor observations Chetrit et al. (2013) obtained in the STN.

A clear limitation of the model is that the oscillations it generates are in the highest part of the β-band, whereas MPTP monkeys rather exhibit oscillations in the lower range (Tachibana et al., 2011). In humans, abnormal oscillations in the STN of PD patients have been measured in both the low- and high-beta ranges (Oswal et al., 2016, 2021). However, the positive effects of dopamine medication or of deep brain stimulation on motor symptoms correlate with a decrease in the power of the low-beta component only (Darcy et al., 2022; Lofredi et al., 2023). The high-beta activity seems to result from cortical inputs rather than from intrinsic BG activity (Oswal et al., 2016, 2021). For all these reasons, it would be expected that the beta oscillations generated by the intrinsic BG circuitry in our model would rather be in the low-beta range. This discrepancy may result from a

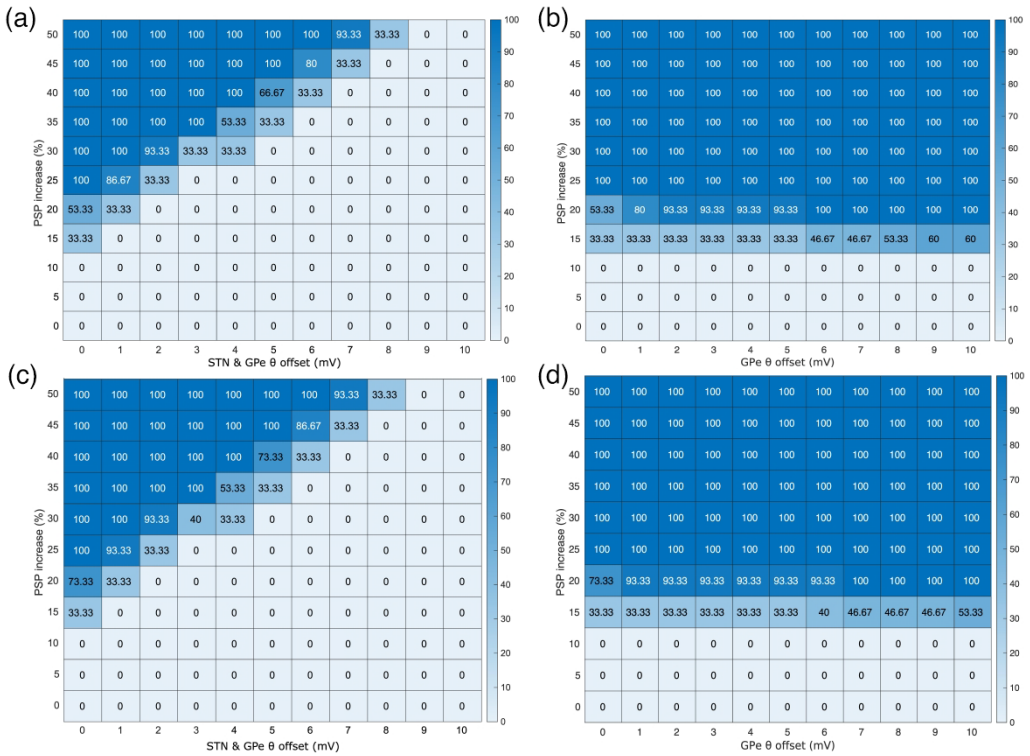

FIGURE 12 Effect of the simulation of D5 receptors in the GPe with regards to the emergence of oscillations under dopamine depletion. (a, b) Using the Cmpr set of delays. (c, d) Using the NoPlkv set of delays. Same as Figure 4a, except that in (a) and (c), θ is increased in both STN and GPe and in (b) and (d), only in the GPe.

number of simplifications. First, the dynamics of the simulated neural populations depend exclusively on the dynamics of the post-synaptic potentials (PSPs) at the synaptic level; no other internal dynamics of the neuron itself are simulated that would dampen the oscillations. Second, only the fast GAGAA inhibitory transmission was simulated, whereas the much slower GABAB has not been simulated and would, on average, slow the inhibitory transmission, especially in the GPe ↔ STN loop. Third, no synaptic adaptation mechanisms were included, whereas Shouno et al. (2017) suggest that short-term facilitation and depression participate in the GPe–STN loop behaviour. Investigating whether these simplifications are sufficient to explain this discrepancy is the matter of future work.

4.2 | Theories of β-band oscillations

There are several theories for the origin of β-band oscillations in the BG: the *striatal origin theory*, based on the hypothesis of changes in intrinsic properties of striatal MSNs (McCarthy et al., 2011); the *striatal inhibition theory* on the increased striatal inhibition by means of the D2 neurons on the GPe–STN loop (Kumar et al., 2011; Lindahl & Hellgren Kotaleski, 2016); and the *FSI loop theory*, which posits that (in mice) the GPe to striatum feedback projection (through the FSI) is the cause of the oscillations (Corbit et al., 2016). When it comes to explaining primate data, these theories have been nevertheless challenged by experimental evidence showing that the GPe still exhibits oscillatory behaviour after having severed its inhibitory inputs from MSN (Tachibana et al., 2011) and by the absence of segregated striato-fugal pathways. Concerning the *FSI loop theory*, our results show that, in primates, the role of the MSN–GPe–FSI loop is consistent with a relay transferring GPe–STN oscillations back to the striatum (see Figures 7 and 8) and that it is unlikely to be a source. Additionally, Van Albada et al. (2009) and Van Albada and Robinson (2009) introduced the hypothesis of the *thalamo-cortical loop* being the primary cause of oscillation. Again, this hypothesis seems unlikely, as (1) it requires the segregation of direct/indirect pathways which is non-existent or partial in primates and (2) it is severely constrained by long intrinsic delays, which are more suitable to sustain θ- than β-band oscillations (Leblois et al., 2006). Finally, Pavlides et al. (2015) showed that it is possible for a properly parameterised cortico-basal model encompassing three loops (the STN ↔ GPe, the intra-cortical and the cortico-basal) to contribute to the emergence of β oscillations, without any of them being capable of autonomously sustaining them.

By contrast to the aforementioned hypotheses and models, our proposal shows that the STN ↔ GPe loop of primates is ready to oscillate autonomously in the β-band by simply increasing the coupling between both nuclei. Furthermore, although previous research had already hinted this loop to be the source of sustained β-band oscillations (Gillies et al., 2002; Terman et al., 2002), we are first to pinpoint the opposing roles of D2 and D5 extrastriate receptors in the emergence of these oscillations.

Together with our results, three other independent studies suggested the GPe–STN loop to be crucial to generate oscillations in the β-band. However, they exhibit some degree of inconsistency with experimental data, either in their assumptions or in their implementation, or rely on additional mechanisms not required in our parsimonious model. First, Tsirogiannis et al. (2010) used unrealistic brief transmission delays (1 ms for both GPe → STN and STN → GPe connections, cf. Table 1), assumed PD to influence the time-course of PSPs and relied on the existence of segregated direct/indirect pathways. Likewise, Nevado Holgado et al. (2010) stressed the importance of the transmission delays in this loop to set the oscillation frequency. However, they assumed PD to yield an unrealistically strong change of synaptic strength (two-fold increase for GPe → GPe, almost four-fold for cortex → STN, almost ten-fold for striatum → GPe and GPe → STN). Finally, in their recent spiking model, Shouno et al. (2017) showed that STN–GPe oscillations could emerge if post-inhibitory rebound excitation at the STN level and short-term plasticity in both STN and GPe were introduced. Our model shows that these mechanisms are nevertheless not required.

Humphries et al. (2006) have shown that GPe–STN oscillations in rats would yield γ-band and slow (<1 Hz) oscillations. To assess the generality of our hypothesis, we transferred the delays of Humphries et al. (2006) to our primate model, to test whether the predicted frequency of our model would also match data obtained experimentally on that species. Interestingly, when changing the transmission delays of our model to those of the rodent literature (namely 4 ms for GPe → STN and 2 ms for STN → GPe), our predicted oscillation frequency shifted to 44 Hz (Figure 9), a value reasonably close to those recorded in rats (53–55 Hz). Although cautiously, this may suggest a common principle of oscillation across both species. Note however that experimental results tend to suggest that the mechanisms of abnormal oscillations in PD models can be different from one species to another: The involvement of the STN reported in monkeys (Tachibana et al., 2011) has not been found in mice (de la Crompe et al., 2020).

5 | METHODS

5.1 | Characterisation of delays between primate BG nuclei

For our model to make sensible predictions about the naturally occurring frequencies of oscillation across BG nuclei, it was first required to establish the typical transmission delays across them for the case of the macaque brain, which are not directly available. Instead, we had to derive them from the latencies between excitatory and inhibitory events recorded during stimulation studies (Iwamuro et al., 2009, 2017; Kita et al., 2004, 2006; Nambu et al., 2000, 2002; Polyakova et al., 2020; Tachibana et al., 2008; Turner & DeLong, 2000; Yoshida et al., 1993). Therefore, it was first necessary to develop a methodology to properly identify the combinations of pathways and transmission delays involved in each experimental data set (see Tables 2, 3 and 4), so as to extract the specific delays across BG nuclei.

To that end, we considered all known connections within the BG (Figure 13a), with the exception of the sparse projections from STN to striatum and from GPe to striatum (Jaeger & Kita, 2011). Indeed, STN stimulation fails to elicit MSN activity (Kita et al., 2005), and although cortical stimulation elicits MSN overactivity, this is not followed by a noticeable second excitation, which would have signaled a rebound mediated by the STN (Nambu et al., 2002). Also, if the GPe to striatum projection were functionally active in stimulation studies, we would expect the subsequent inhibition of the GPe to cause MSN overactivity, an event that has not been observed experimentally (Nambu et al., 2002). Notice that the resulting simplification of the BG connectivity graph is also in line with the results of our previous study (Liénard & Girard, 2014), which showed that the influence of these pathways on the striatum could only be potent if they targeted the FSI. Hence, they could only influence the MSNs by silencing them through interneurons, and as MSNs are already mostly silent at rest, this should not have observable consequences on the other nuclei.

To match the timings between excitatory and inhibitory events reported in the literature, we first deployed the graph of the projections potentially involved in a series of candidate pathways (Figure 13 discussed in the next section). We further trimmed down the number of pathways by excluding highly recurrent ones to lower the computational complexity of the search. We limit in particular the number of iterations through the STN ↔ GPe loop to two, as more iterations would result in latencies that are too long; other exclusions are discussed in detail in the following section 'Pathways involved in the stimulation experiments'. The resulting set of candidate pathways is summarised along with the experimental timing references in Tables 2, 3 and 4. Note that some of the studies we include here stimulated different cortical areas; for example, Nambu et al. (2000) stimulated the primary motor area (M1) as well as the supplementary motor area (SMA). In such cases, we rely on the shortest latency reported per study.

We then perform an exhaustive exploration of the space of axonal delays to find the best fit. In order to achieve this, we compute the time that would be needed by each pathway in a simplified model to match the

TABLE 4 Summary of the candidate pathways and reference data (Part 3).

Stim.	Rec.	Response	Candidate pathways	Latency (ms)
Ctx	GPi	Early exc.	Ctx → Str → GPe → STN → GPi	7.8 ± 2.4[a]
			Ctx → STN → GPi	9.2 ± 2.2[b]
			Ctx → STN → GPe → STN → GPe → GPi	10.0 ± 2.6[c]
		Inhibition	Ctx → Str → GPi	20.9 ± 5.0[a]
				19.4 ± 3.0[b]
				19.4 ± 4.6[c]
				24.6 ± 5.1[d]
		Late exc.	Ctx → Str → GPe → STN → GPi	29.9 ± 6.5[a]
			Ctx → STN → GPi	32.6 ± 8.7[b]
			Ctx → STN → GPe → STN → GPe → GPi	28.2 ± 5.2[c]
			Ctx → STN → GPe → STN → GPe → STN → GPi	

Note: See Table 2 for notations.

[a]Nambu et al. (2000).

[b]Tachibana et al. (2008).

[c]Iwamuro et al. (2017).

[d]Yoshida et al. (1993).

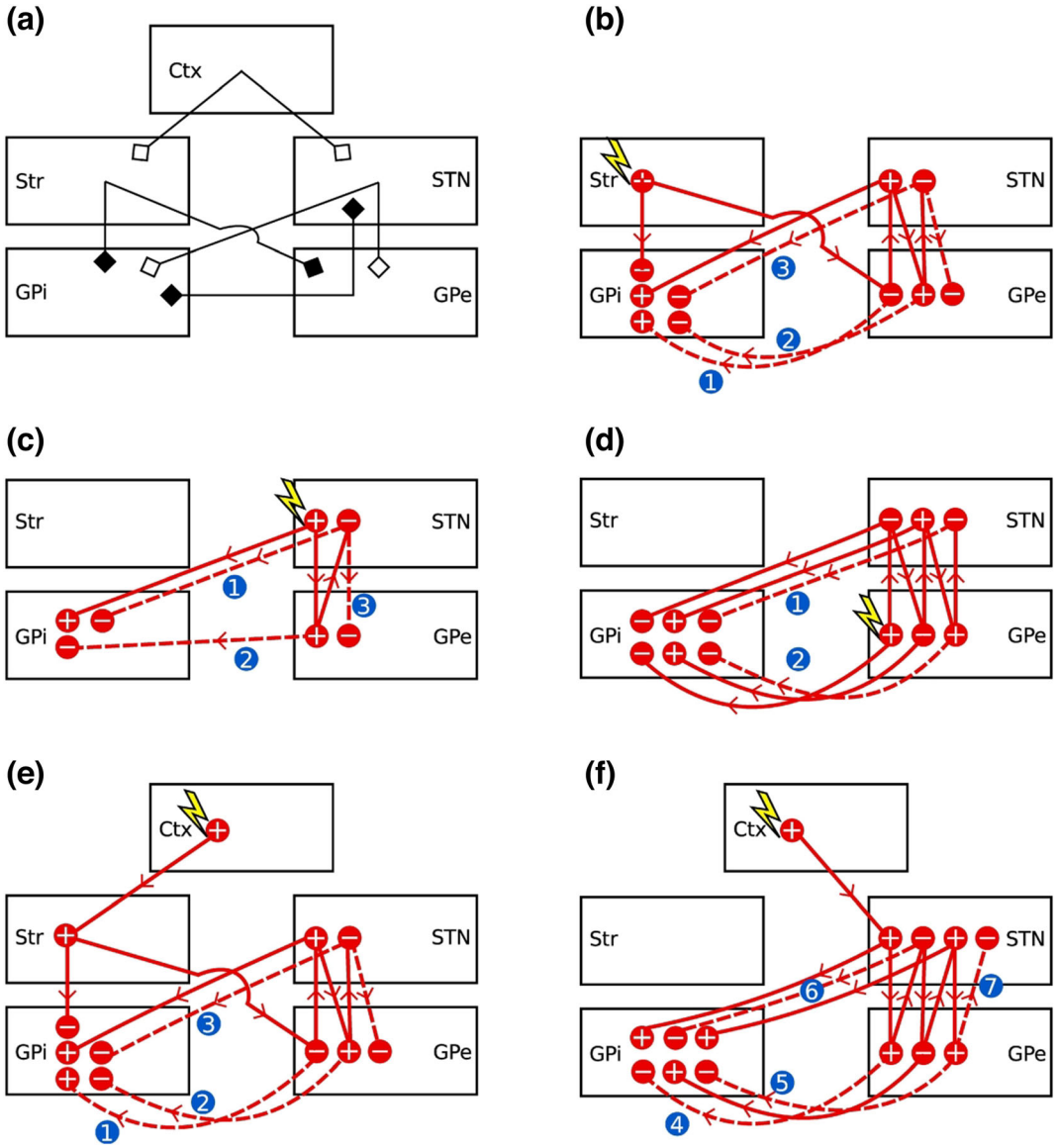

FIGURE 13 (a) Connections considered in the transmission delay estimation. Black endings denote inhibitory connections and white endings denote excitatory connections. (b–f) Possible timecourses of a stimulation originating in the striatum (b), STN (c), GPe (d) and cortex (e, f). For clarity, the cortical stimulation is subdivided into one representation of the striatal excitation consequences (e) and of the subthalamic excitation consequences (f). In all panels, circled '+' indicates overactive nuclei, and '−' indicates underactive nuclei. Successive states of overactivity or underactivity are placed from left to right if they can be ordered (e.g. after an excitation in the Str, the STN will always be overactive before being underactive). Successive states that can not be ordered are placed on different lines (e.g. after an excitation in the Str, the first state of GPi could a priori be either an underactivity or an overactivity). Dashed numbered links correspond to pathways that are not recruited; see text for their individual justifications.

experimentally recorded delay and score the fit of the quickest pathway with experimental data. To aid the optimisation process, all delays were constrained to assume biologically plausible values (1–12 ms). Our exhaustive search to find the optimal fit thus implied the evaluation of all 12^8 (≈430 million) possible combinations. Each combination was assigned a score dependent on the amount of experimental data it was able to replicate.

5.2 | Pathways involved in the stimulation experiments

Stimulations in the cortex, Str, STN or GPe result in an intricate superposition of excitatory and inhibitory effects that could be supported by a multitude of different pathways. We could however simplify the connection graph to rule out several pathways. We will successively review the different stimulation locations, the excitatory or

inhibitory responses that they cause and the pathways that could be mediating these responses (Figure 13a).

First, we considered the case of striatal stimulation (Figure 13b). Following this stimulation, GPe and GPi neurons are first inhibited, then excited (Kita et al., 2006). The artificial blockade of STN eliminates the excitation but does not affect the inhibition (Kita et al., 2006); hence, the STN is required for the excitation. The excitation can thus not possibly be mediated by the (Str → GPe → GPi) chain because it does not involve the required STN, so we can rule out pathway number 1 of Figure 13b. Furthermore, the artificial blockade of STN does not change the timing of the inhibition, so we can also rule out pathway numbers 2 and 3 of Figure 13b because the chains (Str → GPe → STN → GPe → GPi) and (Str → GPe → STN → GPe → STN → GPe → GPi) involve the STN and result in an inhibition of GPi.

Next, we considered a stimulation in the STN (Figure 13c). Following this, more than 80% of the responding neurons in the globus pallidus are excited (Nambu et al., 2000). As this excitation is not followed by an observable inhibition, we can rule out the pathways numbered 1, 2 and 3 of Figure 13c because they would lead to an underactivity either in GPe or GPi.

We then considered the GPe stimulation (Figure 13d). In this experiment, only half of the GPi neurons show an early excitation occurring fast (3.4 ± .9 ms), and they all show later an inhibition that is followed by an excitation (Tachibana et al., 2008). This early excitation can hardly be explained by the BG pathways, because the chains finishing earliest in the GPi, that is (GPe → STN → GPi) and (GPe → GPi), result in inhibition. The (GPe → Str → GPi) chain could possibly account for this early excitation; however, we did not include the GPe → MSN pathway as it does not seem to be involved in these stimulation experiments (cf. the beginning of this section), and furthermore, the latency of this excitation is clearly too fast to be mediated through the slow Str → GPi connection. Finally, as discussed in Tachibana et al. (2008), the early excitation could be mediated by STN axons targeting both the GPe and GPi. As this does account for the fact that only half of GPi neurons respond and as other pathways can not plausibly explain an early excitation that is this fast, we will not consider further this early excitation. We can also rule out the pathways numbered 1 and 2 because they suppose a late inhibition following the reported inhibition and excitation in GPi, and Tachibana et al. (2008) did not report such a late inhibition.

Finally, Figure 13e,f illustrates the case of cortical stimulation. This stimulation leads to three distinct temporal responses in STN, GPe and GPi (Nambu et al., 2000): an early excitation followed by an inhibition and finally a late excitation. To understand the possible timecourses of this cortical stimulation, we subdivided it according to the chains beginning with the direct striatal excitation (Figure 13e) and with the direct subthalamic excitation (Figure 13f). After the artificial blockade of activity in the STN, Nambu et al. (2000) reported that the GPi does not exhibit early or late excitation. We can thus deduce that the STN is required for these excitations, so we can rule out pathway 1 of Figure 13e corresponding to the chain (Ctx → Str → GPe → GPi) because the STN is not involved in it. Nambu et al. (2000) also report that after STN blockade, the GPi exhibits the same inhibition, so we deduce that the STN is not part of the chains leading to an inhibition in GPi and rule out the pathways 2–6, corresponding to the chains involving the STN and resulting in an underactivity in GPi. No late inhibition has been reported in Nambu et al. (2000), so the pattern of activity '−' then '+' then '−' in the STN is not plausible. We hence rule out pathway 7.

5.3 | Optimisation of inter-nuclei delays

To compute the time t needed for the stimulation in 'nucleus 1' to flow over a given chain (nucleus 1 → nucleus 2 → ... → nucleus n) and to be eventually recorded in 'nucleus n', we use a simple formula:

$$t = \Phi + \sum_{i=1}^{n-1} (\delta_{i \to i+1} + \xi), \tag{1}$$

with $\delta_{i \to i+1}$ as the axonal delay between nuclei i and $i + 1$, Φ as the time needed for the stimulation to be effective in nucleus 1 and ξ as the time needed for any nucleus to change its firing rate when receiving the stimulation. The time required for the stimulation to be effectively eliciting action potentials is very small, so we set $\Phi = 1$ ms (a value of $\Phi = 0$ ms was also considered and led to similar results). The time required for the action potential once at the synapse level to be captured by the postsynaptic neuron and to change its potential was considered to be $\xi = 1$ ms, equal for all populations for the sake of simplicity. This latter constant is justified by the shape of the change of intensity after a spike mediated by either AMPA or GABAA, because it is already significant after 1 ms (Destexhe et al., 1998) and is in line with the alpha functions that we used in the BCBG model (Liénard & Girard, 2014).

Although most pathways modelled involve successive action potentials, we also test separately the existence of cortical antidromic activation of pyramidal tract neurons at striatal stimulation sites. Indeed, such activation of

PTN neurons has been observed or hypothesised, resulting then in the direct excitation of the STN through the cortical PTN neurons when stimulating the striatum (Bauswein et al., 1989; Turner & DeLong, 2000). When we model this possibility, we consider that the elicitation of action potentials in cortical neurons is near-instantaneous (Turner & DeLong, 2000), and thus, we do not add extra time for its generation. For example, the antidromic pathway that explains the late excitation of GPe after striatal stimulation, noted (GPe ↞ Str antidromic); Ctx → STN → GPe in Table 2 has a delay computed as if the stimulation was directly originated from the cortical PTN neurons. Its formula then follows the general shape described by Equation 1, that is $t = \Phi + (\delta_{\mathrm{Ctx} \to \mathrm{STN}} + \xi) + (\delta_{\mathrm{STN} \to \mathrm{GPe}} + \xi)$.

As a general rule, each candidate pathway is computed for each response type, and the quickest pathway is assumed to be the one that we observe. The exceptions are the cortical stimulations as they cause an early and a late excitation; in these cases, the quickest excitatory response is assumed to correspond to the early excitation, and the quickest excitatory response after the inhibition is assumed to correspond to the late excitation. Overall, 39 candidate pathways corresponding to 21 couples of stimulation/recorded responses are checked against 45 experimental data. These experimental data are noted as $T_{i,j} \pm \sigma_{i,j}$ with i as the number of the stimulation–response pairs and j as the index of the reference for each pair, as given in Tables 2 and 3. The global score χ of the fit between the timing of selected pathways and the reference data is then computed as follows:

$$\chi = \sum_{i=1}^{21} \left(\sum_{j} \exp\left(\frac{-\left(t_i - T_{i,j}\right)^2}{2\sigma_{i,j}^2} \right) \right) \tag{2}$$

5.4 | Computational model of the BG

In this study, we focus on the oscillatory activity of the BG circuitry at rest. With the exception of the changes described below (transmission delays optimised to fit to experimental studies and simulation of DA depletion on extra-striate receptors), the model that we present here adopts the mathematical formalism and parameters we previously developed (Liénard & Girard, 2014). Briefly, each nucleus of the BG is simulated with a mean-field model incorporating the temporal dynamics of neurotransmitters. Inputs from cortical [cortico-striatal neurons, CSN and pyramidal tract neurons, (PTN)], as well as thalamic afferents [from the centromedian and the parafascicular nuclei (CM/Pf)], are modelled as independent random processes with different average firing rates (Bauswein et al., 1989; Pasquereau et al., 2015; Pasquereau & Turner, 2011; Turner & DeLong, 2000). As in Liénard and Girard (2014), the CSN input was simulated as a Gaussian process centred around 2 Hz, PTN around 15 Hz and CM/Pf around 4 Hz. The simulations presented here were obtained using a standard deviation of 2 Hz, corresponding to a high noise in the neuronal activities. The oscillatory patterns obtained with this noise level were similar to those obtained with a lower standard deviation of .5 Hz.

The parameter search in Liénard and Girard (2014) extended over more than 1000 optimal model parametrisations that were equally maximising the plausibility scores defined in that study. An additional assessment showed that most of the variability in these solutions is small jitter [$<10^{-6}$ in a search space normalised within (0, 1)] around 15 different base solutions. Thus, we restricted our study to these 15 base solutions, as they globally represent the optimal parametrisations of the BG obtained in Liénard and Girard (2014), as we did in Girard et al. (2021).

The structure of the model is very close to the one presented in Liénard and Girard (2014), with the exception of the addition of plausible axonal delays and the simulation of dopamine depletion on extrastriate receptors. We use a population model with mean-field formulation. Although we provide here the basic equations of our model, more details about mean-field models can be found elsewhere (e.g. Deco et al., 2008).

One assumption of mean-field models, commonly referred to as the *diffusion approximation*, is that every neuron receives the same inputs from another population. We can hence express the mean number of incoming spikes with neurotransmitter n per neuron of the population x from population y:

$$\Psi_x^n(t) = \upsilon_{i \leftarrow y} \phi_k\left(t - \tau_{y \to x}\right) \tag{3}$$

with $\nu_{x \leftarrow y}$ as the mean number of synapses in one neuron of population x from axons of population y, $\tau_{y \to x}$ as the axonal delay between population y and x and $\varphi_y (t - \tau_{y \to x})$ as the firing rate of population y at time $t - \tau_{y \to x}$.

Axonal varicosity counts $\nu_{x \leftarrow y}$ is the mean count of synapses in population x that are targeted by axons from population y:

$$\upsilon_{x \leftarrow y} = \frac{P_{y \to x} N_y}{N_x} . \alpha_{y \to x} \tag{4}$$

with N_x and N_y as the neuron counts of populations x and y, $\alpha_{y \to x}$ as the mean axonal varicosity count of neurons of y with an axon targeting neurons of x and $P_{y \to x}$ as the proportion of such neurons in population y.

Mean-field models assume that neurons' firing thresholds follow a Gaussian distribution. The mean firing rate of a population x at time t can then be approximated by

$$\phi_x(t) = \frac{S_x^{max}}{1 + \exp\left(\frac{\theta_x - V_x(t)}{\sigma'}\right)} \tag{5}$$

with $V_x(t)$ as the mean potential at the soma at time t, $S^{\max}{}_x$ as the maximal possible firing rate, θ_x as the mean difference between resting and firing thresholds and, as per Van Albada and Robinson (2009), $\sigma' = \sigma\frac{\sqrt{3}}{\pi}$ (σ being the standard deviation of the firing thresholds).

The PSP change to the membrane potential at the location of the synapse contributed by a single spike is modelled by the alpha function (Rall, 1967):

$$\Delta V_0^n(t) = ADte^{-Dt} \tag{6}$$

where A and D relate to the amplitude and duration of PSP and depend on the neurotransmitter n mediating the spike. They are computed as follows: $A = A_n \exp(1)$ and $D = \exp(1)/D_n$ (Tsirogiannis et al., 2010), using the constants reported in Liénard and Girard (2014).

We also model in a simple way the attenuation of distal dendrites as a function of the soma distance. By modelling the dendritic field as a single-compartment finite cable with sealed-end boundaries condition (Koch, 2005), we can express for population x:

$$\Delta V_{soma}^n(t) = \Delta V_0^n(t)\frac{\cosh(L_x - Z_x)}{\cosh(L_x)} \tag{7}$$

with $\Delta V^n{}_0\,(t)$ the potential change at the synapse, L_x the electrotonic constant of the neurons and Z_x the mean distance of the synaptic receptors along the dendrites. We further express this mean distance as a percentage of L_x: $Z_x = p_x L_x$. The electrotonic constant is then calculated according to (Koch, 2005):

$$L_x = l_x\sqrt{\frac{4}{d_x}\frac{R_i}{R_m}} \tag{8}$$

with R_i the intracellular resistivity, R_m the membrane resistance, l_x the mean maximal dendritic length and d_x the mean diameters of the dendrites along their whole extent for population x.

The mean potential of the neural population, V_x, is finally obtained by integrating the changes of potential caused by incoming spikes over time:

$$V_x(t) = \int_{-\infty}^{t} \sum_{(y,n)} \Psi_x^n(t')\Delta V_{soma}^n(t')dt' \tag{9}$$

where each couple (y, n) represents one afferent population y with spikes mediated by the neurotransmitter n.

The BG dynamics were simulated with a time-step of 10^{-4} ms, as in Liénard and Girard (2014), using a 4th-order Runge–Kutta integration method.

The code of the model is available on GitHub at https://github.com/SN1885A/BCBG-model.

5.5 | Extra-striate DA depletion

We hypothesised that an abnormal activation of extra-striatal DA receptors, combined with lagged activity due to inter-nuclei transmission delays, is the primary cause of β-band oscillations. To test this hypothesis, we focused on modelling the distribution of DA receptors within the GPe and STN only, as these are the only two nuclei that participate in multiple loops within the BG and could possibly cause oscillations. The GPi was disregarded, as it does not form any closed loop within the BG and thus cannot cause oscillations within the BG.

Since D2 receptors in GPe and STN are located at the pre-synaptic level only (Rommelfanger & Wichmann, 2010), we simulated their deactivation by dopamine depletion with an increase of post-synaptic potentials following an incoming spike, as follows:

$$\begin{aligned} A_{AMPA}^{PD} &= \alpha A_{AMPA}^{normal} \\ A_{NMDA}^{PD} &= \alpha A_{NMDA}^{normal} \\ A_{GABA_A}^{PD} &= \alpha A_{GABA_A}^{normal} \end{aligned} \tag{10}$$

where A_{AMPA}, A_{NMDA} and A_{GABAA} are respectively the peak post-synaptic amplitude of a spike mediated by AMPA, NMDA and $GABA_A$; ^{normal} denotes their reference value defined in Liénard and Girard (2014), and ^{PD}, the increased level following DA depletion computed with the factor α ($\alpha \geq 1$).

The STN D1-like receptors are of the D5 sub-type, expressed at post-synaptic sites, and with constitutive activity (Chetrit et al., 2013). They have thus been modelled as modulators of the transfer function of the

STN neuron population (see the next equation), rather than as modulators of incoming activity:

$$\theta_{STN}^{PD} = \Delta_{STN} + \theta_{STN}^{\text{normal}} \quad (11)$$

where θ_{STN} is the average firing threshold of STN neurons, and Δ_{STN} is the offset created by DA depletion on D5 receptors ($\Delta_{\text{STN}} \geq 0$).

Finally, based on the lack of projective selectivity of D1 and D2 MSN in macaque monkeys, we assumed that, on average, they compensate each other and that, consequently, their influence on the emergence of β-band oscillations is non-essential. This simplification constitutes a relatively radical modelling choice that aims at studying the extent to which PD oscillatory phenomenon can be explained without segregated striatal pathways.

5.6 | Code accessibility

The code used to simulate the neural network is available at https://github.com/SN1885A/BCBG-model.

AUTHOR CONTRIBUTIONS

Jean Liénard: Formal analysis; investigation; methodology; software; writing—review and editing. **Lise Aubin:** Formal analysis; investigation; software; writing—review and editing. **Ignasi Cos:** Formal analysis; funding acquisition; investigation; methodology; supervision; writing—original draft; writing—review and editing. **Benoît Girard:** Funding acquisition; methodology; project administration; resources; supervision; writing—original draft; writing—review and editing.

ACKNOWLEDGEMENTS

The authors are grateful for the constructive comments of Mark Humphries in an earlier version of this manuscript. This project was partially funded by the ANR EvoNeuro project, ANR-09-EMER-005-01, as well as by the Laboratory of Excellence SMART (ANR-11-LABX-65), supported by French State funds managed by the ANR within the Investissements d'Avenir programme under reference ANR-11-IDEX-0004-02. Ignasi Cos was funded by the Ville de Paris HABOT Project, the Marie Sklodowska–Curie Research Grant Scheme, grant number IF-656262 and the Serra–Hunter Fellow Program.

CONFLICT OF INTEREST STATEMENT

The authors declare no conflicts of interest.

PEER REVIEW

The peer review history for this article is available at https://www.webofscience.com/api/gateway/wos/peer-review/10.1111/ejn.16271.

DATA AVAILABILITY STATEMENT

The data used in the simulations is included in the code, see code accessibility.

ORCID

Benoît Girard https://orcid.org/0000-0002-8117-7064

REFERENCES

Bauswein, E., Fromm, C., & Preuss, A. (1989). Corticostriatal cells in comparison with pyramidal tract neurons: Contrasting properties in the behaving monkey. *Brain Research*, *493*(1), 198–203. https://doi.org/10.1016/0006-8993(89)91018-4

Bellinger, S., Miyazawa, G., & Steinmetz, P. (2008). Submyelin potassium accumulation may functionally block subsets of local axons during deep brain stimulation: A modeling study. *Journal of Neural Engineering*, *5*(3), 263–274. https://doi.org/10.1088/1741-2560/5/3/001

Benazzouz, A., Mamad, O., Abedi, P., Bouali-Benazzouz, R., & Chetrit, J. (2014). Involvement of dopamine loss in extrastriatal basal ganglia nuclei in the pathophysiology of Parkinson's disease. *Frontiers in Aging Neuroscience*, *6*, 87. https://doi.org/10.3389/fnagi.2014.00087

Brittain, J.-S., & Brown, P. (2014). Oscillations and the basal ganglia: Motor control and beyond. *NeuroImage*, *85*, 637–647. https://doi.org/10.1016/j.neuroimage.2013.05.084

Chen, W., de Hemptinne, C., Miller, A. M., Leibbrand, M., Little, S. J., Lim, D. A., Larson, P. S., & Starr, P. A. (2020). Prefrontal-subthalamic hyperdirect pathway modulates movement inhibition in humans. *Neuron*, *106*(4), 579–588. https://doi.org/10.1016/j.neuron.2020.02.012

Chetrit, J., Taupignon, A., Froux, L., Morin, S., Bouali-Benazzouz, R., Naudet, F., Kadiri, N., Gross, C. E., Bioulac, B., & Benazzouz, A. (2013). Inhibiting subthalamic d5 receptor constitutive activity alleviates abnormal electrical activity and reverses motor impairment in a rat model of Parkinson's disease. *The Journal of Neuroscience*, *33*(37), 14840–14849. https://doi.org/10.1523/JNEUROSCI.0453-13.2013

Corbit, V. L., Whalen, T. C., Zitelli, K. T., Crilly, S. Y., Rubin, J. E., & Gittis, A. H. (2016). Pallidostriatal projections promote β oscillations in a dopamine-depleted biophysical network model. *Journal of Neuroscience*, *36*(20), 5556–5571. https://doi.org/10.1523/JNEUROSCI.0339-16.2016

Darcy, N., Lofredi, R., Al-Fatly, B., Neumann, W.-J., Hübl, J., Brücke, C., Krause, P., Schneider, G.-H., & Kühn, A. (2022). Spectral and spatial distribution of subthalamic beta peak activity in Parkinson's disease patients. *Experimental Neurology*, *356*, 114150. https://doi.org/10.1016/j.expneurol.2022.114150

de la Crompe, B., Aristieta, A., Leblois, A., Elsherbiny, S., Boraud, T., & Mallet, N. P. (2020). The globus pallidus orchestrates abnormal network dynamics in a model of Parkinsonism. *Nature Communications*, *11*(1), 1570. https://doi.org/10.1038/s41467-020-15352-3

Deco, G., Jirsa, V., Robinson, P., Breakspear, M., & Friston, K. (2008). The dynamic brain: From spiking neurons to neural masses and cortical fields. *PLoS Computational Biology*, *4*(8), e1000092. https://doi.org/10.1371/journal.pcbi.1000092

Destexhe, A., Mainen, Z., & Sejnowski, T. (1998). Kinetic models of synaptic transmission. *Methods in Neuronal Modeling*, *2*, 1–25.

Gatev, P., Darbin, O., & Wichmann, T. (2006). Oscillations in the basal ganglia under normal conditions and in movement disorders. *Movement Disorders*, *21*(10), 1566–1577. https://doi.org/10.1002/mds.21033

Gillies, A., Willshaw, D., & Li, Z. (2002). Subthalamic–pallidal interactions are critical in determining normal and abnormal functioning of the basal ganglia. *Proceedings of the Biological Sciences*, *269*, 545–551.

Girard, B., Aubin, L., & Liénard, J. F. (2024). Transmission delays and oscillations in the basal ganglia. figshare. https://doi.org/10.6084/m9.figshare.21131911.v1

Girard, B., Lienard, J., Gutierrez, C. E., Delord, B., & Doya, K. (2021). A biologically constrained spiking neural network model of the primate basal ganglia with overlapping pathways exhibits action selection. *European Journal of Neuroscience*, *53*(7), 2254–2277. https://doi.org/10.1111/ejn.14869

Goldberg, J., Boraud, T., Maraton, S., Haber, S., Vaadia, E., & Bergman, H. (2002). Enhanced synchrony among primary motor cortex neurons in the 1-methyl-4-phenyl-1, 2, 3, 6-tetrahydropyridine primate model of Parkinson's disease. *The Journal of Neuroscience*, *22*(11), 4639–4653. https://doi.org/10.1523/JNEUROSCI.22-11-04639.2002

Guilhemsang, L., & Mallet, N. P. (2024). Arkypallidal neurons in basal ganglia circuits: Unveiling novel pallidostriatal loops? *Current Opinion in Neurobiology*, *84*, 102814. https://doi.org/10.1016/j.conb.2023.102814

Holgado, A., Terry, J., & Bogacz, R. (2010). Conditions for the generation of beta oscillations in the subthalamic nucleus–globus pallidus network. *The Journal of Neuroscience*, *30*(37), 12340–12352. https://doi.org/10.1523/JNEUROSCI.0817-10.2010

Humphries, M., Stewart, R., & Gurney, K. (2006). A physiologically plausible model of action selection and oscillatory activity in the basal ganglia. *The Journal of Neuroscience*, *26*(50), 12921–12942. https://doi.org/10.1523/JNEUROSCI.3486-06.2006

Iwamuro, H., Tachibana, Y., Saito, N., & Nambu, A. (2009). Organization of motor cortical inputs to the subthalamic nucleus in the monkey. In H. Groenewegen, P. Voorn, H. Berendse, A. Mulder, & A. Cools (Eds.), *The Basal Ganglia IX*. Advances in Behavioral Biology (Vol. 58). Springer. https://doi.org/10.1007/978-1-4419-0340-2_9

Iwamuro, H., Tachibana, Y., Ugawa, Y., Saito, N., & Nambu, A. (2017). Information processing from the motor cortices to the subthalamic nucleus and globus pallidus and their somatotopic organizations revealed electrophysiologically in monkeys. *European Journal of Neuroscience*, *46*(11), 2684–2701. https://doi.org/10.1111/ejn.13738

Jaeger, D., & Kita, H. (2011). Functional connectivity and integrative properties of globus pallidus neurons. *Neuroscience*, *198*, 44–53. https://doi.org/10.1016/j.neuroscience.2011.07.050

Katabi, S., Adler, A., Deffains, M., & Bergman, H. (2023). Dichotomous activity and function of neurons with low- and high-frequency discharge in the external globus pallidus of non-human primates. *Cell Reports*, *42*(1), 111898. https://doi.org/10.1016/j.celrep.2022.111898

Kita, H., Chiken, S., Tachibana, Y., & Nambu, A. (2006). Origins of $GABA_A$ and $GABA_B$ receptor-mediated responses of globus pallidus induced after stimulation of the putamen in the monkey. *The Journal of Neuroscience*, *26*(24), 6554–6562. https://doi.org/10.1523/JNEUROSCI.1543-06.2006

Kita, H., Nambu, A., Kaneda, K., Tachibana, Y., & Takada, M. (2004). Role of ionotropic glutamatergic and gabaergic inputs on the firing activity of neurons in the external pallidum in awake monkeys. *Journal of Neurophysiology*, *92*(5), 3069–3084. https://doi.org/10.1152/jn.00346.2004

Kita, H., Tachibana, Y., Nambu, A., & Chiken, S. (2005). Balance of monosynaptic excitatory and disynaptic inhibitory responses of the globus pallidus induced after stimulation of the subthalamic nucleus in the monkey. *The Journal of Neuroscience*, *25*(38), 8611–8619. https://doi.org/10.1523/JNEUROSCI.1719-05.2005

Koch, C. (2005). *Biophysics of computation: Information processing in single neurons*. Oxford University Press.

Koshimizu, Y., Fujiyama, F., Nakamura, K. C., Furuta, T., & Kaneko, T. (2013). Quantitative analysis of axon bouton distribution of subthalamic nucleus neurons in the rat by single neuron visualization with a viral vector. *Journal of Comparative Neurology*, *521*(9), 2125–2146. https://doi.org/10.1002/cne.23277

Kumar, A., Cardanobile, S., Rotter, S., & Aertsen, A. (2011). The role of inhibition in generating and controlling Parkinson's disease oscillations in the basal ganglia. *Frontiers in Systems Neuroscience*, *5*, 86. https://doi.org/10.3389/fnsys.2011.00086

Leblois, A., Boraud, T., Meissner, W., Bergman, H., & Hansel, D. (2006). Competition between feedback loops underlies normal and pathological dynamics in the basal ganglia. *The Journal of Neuroscience*, *26*(13), 3567–3583. https://doi.org/10.1523/JNEUROSCI.5050-05.2006

Lévesque, M., & Parent, A. (2005). The striatofugal fiber system in primates: A reevaluation of its organization based on single-axon tracing studies. *Proceedings of the National Academy of Sciences*, *102*(33), 11888–11893. https://doi.org/10.1073/pnas.0502710102

Liénard, J., & Girard, B. (2014). A biologically constrained model of the whole basal ganglia addressing the paradoxes of connections and selection. *Journal of Computational Neuroscience*, *36*(3), 445–468. https://doi.org/10.1007/s10827-013-0476-2

Lindahl, M., & Hellgren Kotaleski, J. (2016). Untangling basal ganglia network dynamics and function: Role of dopamine depletion and inhibition investigated in a spiking network model. *eNeuro*, *3*(6), e0156–16.2016.

Lofredi, R., Okudzhava, L., Irmen, F., Brücke, C., Huebl, J., Krauss, J. K., Schneider, G.-H., Faust, K., Neumann, W.-J., & Kühn, A. A. (2023). Subthalamic beta bursts correlate with dopamine-dependent motor symptoms in 106 Parkinson's patients. *NPJ Parkinson's Disease*, *9*(1), 2. https://doi.org/10.1038/s41531-022-00443-3

McCarthy, M., Moore-Kochlacs, C., Gu, X., Boyden, E., Han, X., & Kopell, N. (2011). Striatal origin of the pathologic beta oscillations in Parkinson's disease. *Proceedings of the National*

Academy of Sciences, *108*(28), 11620–11625. https://doi.org/10.1073/pnas.1107748108

Nadjar, A., Brotchie, J., Guigoni, C., Li, Q., Zhou, S., Wang, G., Ravenscroft, P., Georges, F., Crossman, A., & Bezard, E. (2006). Phenotype of striatofugal medium spiny neurons in parkinsonian and dyskinetic nonhuman primates: A call for a reappraisal of the functional organization of the basal ganglia. *The Journal of Neuroscience*, *26*(34), 8653–8661. https://doi.org/10.1523/JNEUROSCI.2582-06.2006

Nambu, A., Kaneda, K., Tokuno, H., & Takada, M. (2002). Organization of corticostriatal motor inputs in monkey putamen. *Journal of Neurophysiology*, *88*(4), 1830–1842. https://doi.org/10.1152/jn.2002.88.4.1830

Nambu, A., Tokuno, H., Hamada, I., Kita, H., Imanishi, M., Akazawa, T., Ikeuchi, Y., & Hasegawa, N. (2000). Excitatory cortical inputs to pallidal neurons via the subthalamic nucleus in the monkey. *Journal of Neurophysiology*, *84*(1), 289–300. https://doi.org/10.1152/jn.2000.84.1.289

Oswal, A., Beudel, M., Zrinzo, L., Limousin, P., Hariz, M., Foltynie, T., Litvak, V., & Brown, P. (2016). Deep brain stimulation modulates synchrony within spatially and spectrally distinct resting state networks in Parkinson's disease. *Brain*, *139*(5), 1482–1496. https://doi.org/10.1093/brain/aww048

Oswal, A., Cao, C., Yeh, C.-H., Neumann, W.-J., Gratwicke, J., Akram, H., Horn, A., Li, D., Zhan, S., Zhang, C., Wang, Q., Zrinzo, L., Foltynie, T., Limousin, P., Bogacz, R., Sun, B., Husain, M., Brown, P., & Litvak, V. (2021). Neural signatures of hyperdirect pathway activity in Parkinson's disease. *Nature Communications*, *12*(1), 5185. https://doi.org/10.1038/s41467-021-25366-0

Parent, A., Charara, A., & Pinault, D. (1995). Single striatofugal axons arborizing in both pallidal segments and in the substantia nigra in primates. *Brain Research*, *698*(1), 280–284. https://doi.org/10.1016/0006-8993(95)01017-P

Pasquereau, B., DeLong, M. R., & Turner, R. S. (2015). Primary motor cortex of the parkinsonian monkey: Altered encoding of active movement. *Brain*, *139*(1), 127–143.

Pasquereau, B., & Turner, R. (2011). Primary motor cortex of the parkinsonian monkey: Differential effects on the spontaneous activity of pyramidal tract-type neurons. *Cerebral Cortex*, *21*(6), 1362–1378. https://doi.org/10.1093/cercor/bhq217

Pavlides, A., Hogan, S. J., & Bogacz, R. (2015). Computational models describing possible mechanisms for generation of excessive beta oscillations in Parkinson's disease. *PLoS Computational Biology*, *11*(12), e1004609. https://doi.org/10.1371/journal.pcbi.1004609

Polyakova, Z., Chiken, S., Hatanaka, N., & Nambu, A. (2020). Cortical control of subthalamic neuronal activity through the hyperdirect and indirect pathways in monkeys. *Journal of Neuroscience*, *40*(39), 7451–7463. https://doi.org/10.1523/JNEUROSCI.0772-20.2020

Rall, W. (1967). Distinguishing theoretical synaptic potentials computed for different soma-dendritic distributions of synaptic input. *Journal of Neurophysiology*, *30*(5), 1138–1168. https://doi.org/10.1152/jn.1967.30.5.1138

Rommelfanger, K. S., & Wichmann, T. (2010). Extrastriatal dopaminergic circuits of the basal ganglia. *Frontiers in Neuroanatomy*, *4*, 139. https://doi.org/10.3389/fnana.2010.00139

Shouno, O., Tachibana, Y., Nambu, A., & Doya, K. (2017). Computational model of recurrent subthalamo-pallidal circuit for generation of parkinsonian oscillations. *Frontiers in Neuroanatomy*, *11*(21), 21. https://doi.org/10.3389/fnana.2017.00021

Tachibana, Y., Iwamuro, H., Kita, H., Takada, M., & Nambu, A. (2011). Subthalamo-pallidal interactions underlying parkinsonian neuronal oscillations in the primate basal ganglia. *European Journal of Neuroscience*, *34*(9), 1470–1484. https://doi.org/10.1111/j.1460-9568.2011.07865.x

Tachibana, Y., Kita, H., Chiken, S., Takada, M., & Nambu, A. (2008). Motor cortical control of internal pallidal activity through glutamatergic and gabaergic inputs in awake monkeys. *European Journal of Neuroscience*, *27*(1), 238–253. https://doi.org/10.1111/j.1460-9568.2007.05990.x

Terman, D., Rubin, J., Yew, A., & Wilson, C. (2002). Activity patterns in a model for the subthalamopallidal network of the basal ganglia. *The Journal of Neuroscience*, *22*(7), 2963–2976. https://doi.org/10.1523/JNEUROSCI.22-07-02963.2002

Tsirogiannis, G., Tagaris, G., Sakas, D., & Nikita, K. (2010). A population level computational model of the basal ganglia that generates parkinsonian local field potential activity. *Biological Cybernetics*, *102*(2), 155–176. https://doi.org/10.1007/s00422-009-0360-3

Turner, R., & DeLong, M. (2000). Corticostriatal activity in primary motor cortex of the macaque. *The Journal of Neuroscience*, *20*(18), 7096–7108. https://doi.org/10.1523/JNEUROSCI.20-18-07096.2000

Van Albada, S., & Robinson, P. (2009). Mean-field modeling of the basal ganglia-thalamocortical system. I. Firing rates in healthy and parkinsonian states. *Journal of Theoretical Biology*, *257*(4), 642–663. https://doi.org/10.1016/j.jtbi.2008.12.018

Van Albada, S. J., Gray, R., Drysdale, P., & Robinson, P. (2009). Mean-field modeling of the basal ganglia–thalamocortical system. II dynamics of parkinsonian oscillations. *Journal of Theoretical Biology*, *257*(4), 664–688. https://doi.org/10.1016/j.jtbi.2008.12.013

Yelnik, J., & Percheron, G. (1979). Subthalamic neurons in primates: A quantitative and comparative analysis. *Neuroscience*, *4*(11), 1717–1743. https://doi.org/10.1016/0306-4522(79)90030-7

Yoshida, S., Nambu, A., & Jinnai, K. (1993). The distribution of the globus pallidus neurons with input from various cortical areas in the monkeys. *Brain Research*, *611*(1), 170–174. https://doi.org/10.1016/0006-8993(93)91791-P

How to cite this article: Liénard, J. F., Aubin, L., Cos, I., & Girard, B. (2024). Estimation of the transmission delays in the basal ganglia of the macaque monkey and subsequent predictions about oscillatory activity under dopamine depletion. *European Journal of Neuroscience*, 1–24. https://doi.org/10.1111/ejn.16271